A&A 573, A70 (2015)
DOI: 10.1051/0004-6361/201424117
© ESO 2014

Astronomy & Astrophysics

Observing multiple stellar populations with VLT/FORS2

Main sequence photometry in outer regions of NGC 6752, NGC 6397, and NGC 6121 (M 4)⋆,⋆⋆

D. Nardiello[1,2,3], A. P. Milone[2], G. Piotto[1,3], A. F. Marino[2], A. Bellini[4], and S. Cassisi[5]

[1] Dipartimento di Fisica e Astronomia "Galileo Galilei", Università di Padova, Vicolo dell'Osservatorio 3, 35122 Padova, Italy
e-mail: domenico.nardiello@studenti.unipd.it, giampaolo.piotto@unipd.it
[2] Research School of Astronomy and Astrophysics, The Australian National University, Cotter Road, 2611 Weston, ACT, Australia
e-mail: [antonino.milone; anna.marino]@anu.edu.au
[3] INAF – Osservatorio Astronomico di Padova, Vicolo dell'Osservatorio 5, 35122 Padova, Italy
[4] Space Telescope Science Institute, 3700 San Martin Dr., Baltimore, MD 21218, USA
e-mail: bellini@stsci.edu
[5] INAF – Osservatorio Astronomico di Collurania, via M. Maggini, 64100 Teramo, Italy
e-mail: cassisi@oa-teramo.inaf.it

Received 2 May 2014 / Accepted 23 October 2014

ABSTRACT

Aims. We present the photometric analysis of the external regions of three Galactic globular clusters: NGC 6121, NGC 6397, and NGC 6752. The main goal is the characterization of multiple stellar populations along the main sequence (MS) and the study of the radial trend of different populations hosted by the target clusters.
Methods. The data have been collected using the FOcal Reducer and low dispersion Spectrograph 2 (FORS2) mounted at the Very Large Telescope (VLT) UT1 of the European Southern Observatory (ESO) in $UBVI$ filters. From these data sets we extracted high-accuracy photometry and constructed color–magnitude diagrams (CMDs). We exploit appropriate combinations of colors and magnitudes, which are powerful tools for identifying multiple stellar populations, such as B versus $U-B$ and V versus $c_{U,B,I} = (U-B)-(B-I)$ CMDs.
Results. We confirm previous findings of a split MS in NGC 6752 and NGC 6121. Apart from the extreme case of ω Centauri, this is the first detection of multiple MS from ground-based photometry. For NGC 6752 and NGC 6121, we compare the number ratio of the blue MS to the red MS in the cluster outskirts with the fraction of first and second generation stars measured in the central regions. There is no evidence for significant radial trend.
The MS of NGC 6397 is consistent with a simple stellar population. We propose that the lack of multiple sequences is due both to observational errors and to the limited sensitivity of U, B, V, I photometry to multiple stellar populations in metal-poor GCs.
Finally, we compute the helium abundance for the stellar populations hosted by NGC 6121 and NGC 6752, finding a mild ($\Delta Y \sim 0.02$) difference between stars in the two sequences.

Key words. globular clusters: individual: NGC 6752 – globular clusters: general – globular clusters: individual: NGC 6397 – globular clusters: individual: M 4

1. Introduction

In recent years, the discovery that the color–magnitude diagrams (CMDs) of many globular clusters (GCs) are made of multiple sequences has provided overwhelming proof that these stellar systems have experienced a complex star-formation history. The evidence that GCs host multiple stellar populations has reawakened interest in these objects both from the observational and theoretical point of view.

Multiple sequences have been observed over the entire CMD, from the main sequence (MS, e.g., Piotto et al. 2007) through the subgiant branch (SGB, e.g., Piotto et al. 2012) and from the SGB to the red giant branch (RGB, e.g., Marino et al. 2008), and even in the white dwarf cooling sequence (Bellini et al. 2013a).

Multiple populations along the RGB have been widely studied in a large number of GCs (e.g., Yong et al. 2008; Lee et al. 2009; Monelli et al. 2013) using photometry from both ground-based facilities and from the *Hubble* Space Telescope (HST). In contrast, with the remarkable exception of ω Centauri (Sollima et al. 2007; Bellini et al. 2009b), the investigation of multiple MSs has been carried out with HST only (e.g., Bedin et al. 2004; Piotto et al. 2007; Milone et al. 2012a and references therein; Bellini et al. 2013b).

We will exploit the FOcal Reducer and low dispersion Spectrograph 2 (FORS2), mounted at the Very Large Telescope (VLT) of the European Southern Observatory (ESO) to obtain accurate U, B, V, I photometry of MS stars in the outskirts of

⋆ Based on observations at the European Southern Observatory using the Very Large Telescope on Cerro Paranal through ESO programme 089.D-0978 (P. I. G. Piotto).
⋆⋆ Catalogs of photometry for all globular clusters presented are only available at the CDS via anonymous ftp to cdsarc.u-strasbg.fr (130.79.128.5) or via http://cdsarc.u-strasbg.fr/viz-bin/qcat?J/A+A/573/A70

three nearby GCs, namely NGC 6121 (M 4), NGC 6397, and NGC 6752, and we aim to study their stellar populations.

The paper is organized as follows: in Sect. 2 we provide an overview of the three GCs we studied. The observations and data reduction are described in Sect. 3. The CMDs are analyzed in Sect. 4, where we also show evidence of bimodal MSs for stars in the outskirts of NGC 6121 and NGC 6752 and calculate the fraction of stars in each MS. In Sect. 5, we study the radial distribution of stellar populations in NGC 6752 and NGC 6121. In Sect. 6, we estimate the helium difference between the two stellar populations of NGC 6121 and NGC 6752. A summary follows in Sect. 7.

2. Properties of the target GCs

Multiple stellar populations have been widely studied in the three GCs analyzed here. In this section, we summarize the observational scenario and provide useful information to interpret our observations.

2.1. NGC 6121

NGC 6121 is the closest GC ($d \sim 2.2$ kpc) and has intermediate metal abundance ([Fe/H] = −1.16 Harris 1996, 2010 edition).

The RGB stars of this cluster exhibit a large spread in the abundance distribution of some light-elements such as C, N, O, Na, and Al (Gratton et al. 1986; Brown et al. 1990; Drake et al. 1992; Smith & Briley 2005). There is evidence of a CN bimodality distribution and Na-O anticorrelation (e.g., Norris 1981; Ivans et al. 1999).

The distribution of sodium and oxygen is also bimodal. Sodium-rich (oxygen-poor) stars define a red sequence along the RGB in the U versus $U - B$ CMD, while Na-poor stars populate a bluer RGB sequence (Marino et al. 2008). Further evidence of multiple sequences along the RGB of NGC 6121 are provided by Lee et al. (2009) and Monelli et al. (2013). NGC 6121 has a bimodal HB, populated both on the blue and red side of the instability strip. The HB morphology of this cluster is closely connected with multiple stellar populations. Indeed, blue HB stars are all Na-rich and O-poor (hence belong to the second stellar generation), while red-HB stars have the same chemical composition as first-generation stars (Marino et al. 2011).

2.2. NGC 6397

Located at a distance of 2.3 kpc, NGC 6397 is a very metal-poor GC ([Fe/H] = −2.02; Harris 1996, 2010 edition).

In the late 1970s, Bell et al. (1979) already demonstrated that the RGB stars of this cluster show a spread in light-element abundance. NGC 6397 exhibits modest star-to-star variations of oxygen and sodium and a mild Na-O anticorrelation (e.g., Ramírez & Cohen 2002; Carretta et al. 2009). Similar to NGC 6121, the distribution of sodium and oxygen is bimodal and the groups of Na-rich (O-poor) and Na-poor (O-rich) stars populate two distinct RGBs in the Strömgren y versus c_y index diagram (Lind et al. 2011).

The MS of NGC 6397 is also bimodal, but the small color separation between the two MSs can be detected only when appropriate filters (like the *F225W*, *F336W* from HST/WFC3) are used. Observations of the double MSs from multiwavelength HST photometry have been interpreted as two stellar populations with different light-element abundance and a modest helium variation of $\Delta Y \sim 0.01$ (di Criscienzo et al. 2010; Milone et al. 2012a).

2.3. NGC 6752

NGC 6752 is a nearby metal-poor GC ($d = 4.0$ kpc, [Fe/H] = −1.54; Harris 1996, 2010 edition).

Since the 1980s spectroscopic data reported "anomalies" in the light-element abundances of the RGB stars of this cluster (Norris et al. 1981; Cottrell & Da Costa 1981). More recent works confirm star-to-star light-element variations in NGC 6752 (Grundahl et al. 2002; Yong et al. 2003, 2008, 2013; Carretta et al. 2005), O-Na, Mg-Al, and C-N (anti)correlations for both unevolved (Gratton et al. 2001; Shen et al. 2010; Pancino et al. 2010) and RGB stars (Yong et al. 2005; Carretta et al. 2007, 2012) in close analogy with what was observed in most Galactic GCs (see e.g. Ramírez & Cohen 2002; Carretta et al. 2009 and references therein). In particular, there are three main groups of stars with different Na, O, N, Al, which populate three different RGBs when appropriate indices are used (like the c_1 and c_y Stromgren indices or the $c_{U,B,I}$ visual index; Yong et al. 2008; Yong et al. 2003; Carretta et al. 2012; Monelli et al. 2013).

As shown by Milone et al. (2013, hereafter Mi13), the CMD of NGC 6752 is made of three distinct sequences that can be followed continuously from the MS to the SGB and from the SGB to the RGB. These sequences correspond to three stellar populations with different light-element and helium abundance.

3. Observations and data reduction

We used 2 × 2 binned images taken with the ESO/FORS2 (2 × 2k × 4k MIT CCDs) mounted at the VLT, using the standard resolution collimator. With this configuration, the field of view of FORS2 is reduced to ∼6.′8 × 6.′8 by the MOS unit in the focal plane and the pixel scale is ∼0.″25/pixel. The dithered images of NGC 6121, NGC 6397, and NGC 6752 were acquired using u_HIGH, b_HIGH, v_HIGH, and I_Bessel broadband filters between April 14, 2012 and July 23, 2012. A detailed log of observations is reported in Table 1. Figure 1 shows the combined field of view for each cluster.

We used a modified version of the software described in Anderson et al. (2006) to reduce the data. Briefly, for each image we obtained a grid of 18 empirical point spread functions (PSFs, an array of 3 × 3 PSFs for each chip of FORS2) that vary spatially, using the most isolated, bright and not saturated stars. In this way, each pixel of the image corresponds to a PSF that is a bilinear interpolation of the closest four PSFs of the grid. This makes it possible to measure star positions and fluxes in each individual exposure using an appropriate PSF and to obtain a catalog of stars for each frame. We registered, for each cluster and for each filter, all star positions and magnitudes of each catalog into a common frame (master-frame) using linear transformations. The final result is a list of stars (master list) for each cluster. We plot in Fig. 2 the rms of the photometric residual and of the position as a function of the mean magnitude for each filter and each star measured in NGC 6121. In the case of NGC 6752 and NGC 6397, the distributions are similar.

We specify here that we used magnitude to express the luminosities of the stars under study.

We noted that all the CMDs of the three GCs showed unusually spread out sequences (see panel (a) of Fig. 3 for an example of the V versus $U - V$ CMD of NGC 6397). Part of this spread is due to differential reddening, but this is not the only

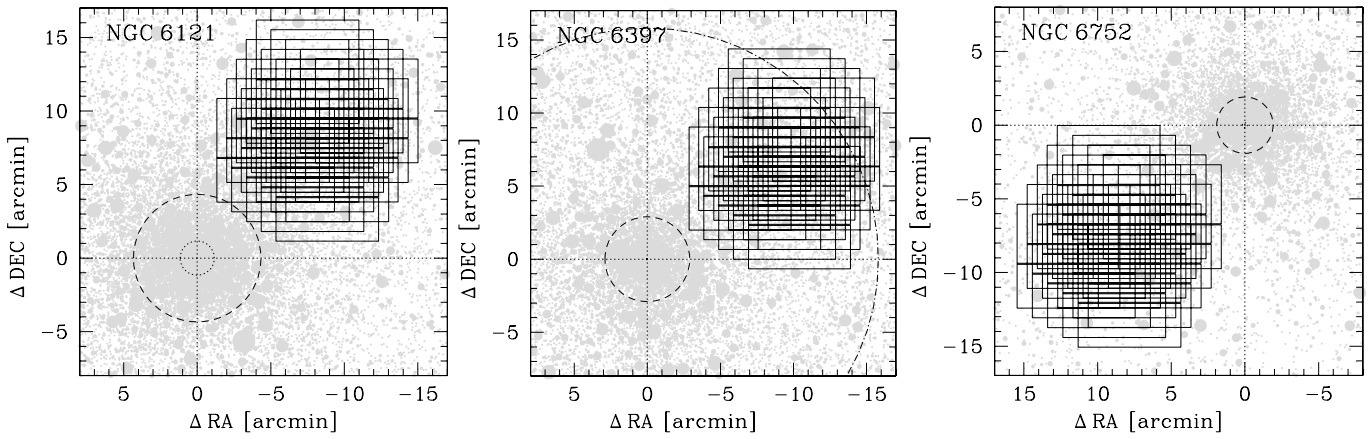

Fig. 1. Dither pattern of the FORS2 images taken in the fields of NGC 6121 (*left*), NGC 6397 (*middle*), and NGC 6752 (*right*). The dotted, dashed, and dashed-dotted circles indicate the core, half-light, and tidal radius of the three GCs. NGC 6397 and NGC 6752 are both post-core-collapse clusters.

Table 1. Log of observations.

Filter	Exp. time	Airmass (s z)	Seeing (arcsec)
	NGC 6121		
u_HIGH	25×410 s	1.004–1.104	0.″58–0.″90
b_HIGH	25×200 s	1.007–1.113	0.″71–1.″20
v_HIGH	25×52 s	1.118–1.251	0.″70–1.″21
I_BESS	25×30 s	1.036–1.150	0.″56–1.″03
	NGC 6397		
u_HIGH	25×410 s	1.153–1.452	0.″81–1.″09
b_HIGH	35×200 s	1.144–1.599	0.″73–1.″52
v_HIGH	50×52 s	1.142–1.272	0.″82–1.″23
I_BESS	25×30 s	1.251–1.355	0.″70–1.″21
	NGC 6752		
u_HIGH	25×410 s	1.227–1.416	0.″67–1.″30
b_HIGH	33×200 s	1.227–1.850	0.″49–1.″36
v_HIGH	25×52 s	1.367–1.483	0.″68–0.″86
I_BESS	25×30 s	1.293–1.363	0.″50–0.″77

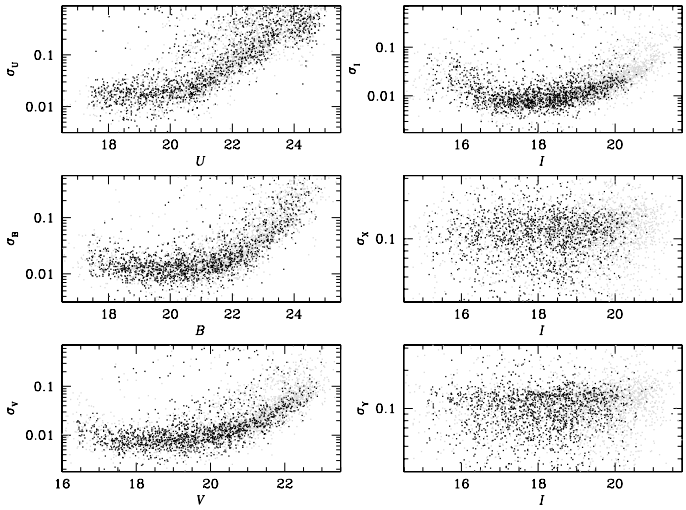

Fig. 2. Photometric (*left panels* and *top right panel*) and position residuals (*middle* and *bottom right panels*) from single measurements in the single images of NGC 6121 plotted as a function of the average magnitude. Gray points show all detected stars; black points refer to proper motion selected stars. In the case of NGC 6752 and NGC 6397, the distributions are similar.

cause. In fact, we found that by selecting stars in different regions of the master list, we obtained shifted MSs. As an example, in panel (d) of Fig. 3, we show the variation of the color $\Delta(U - V)$ for NGC 6397. This plot shows that there is an important gradient of $\Delta(U - V)$ along the x-axis. We selected two groups of stars in this plot : the stars with $x > 1050$ and those with $x < 1050$. We plotted these two subsamples in the V versus $U - V$ CMDs, in black crosses ($x > 1050$) and red circles ($x < 1050$) respectively: panel (a) of Fig. 3 shows the result. The two groups form two shifted MSs. This effect is present in all the CMD of the three GCs, even when they have different extent levels.

Freudling et al. (2007) showed that there is an illumination gradient in the FORS2 flats produced by the twilight sky. This gradient changes with time and with the position of the Sun relative to the pointing of the telescope and could produce a photometric zero-point variation across the FORS2 detectors. The illumination gradient in the flat fields could contribute to the observed enlargement of the CMDs.

We obtained star fluxes using local sky values, and therefore it is expected that these systematic effects are negligible. If the gradient in the flat field images is not properly removed during the prereduction procedure, the pixel quantum efficiency correction will be wrong. The consequence is that the luminosity of a star measured in a given location of the CCD will be underestimated (or overestimated) with respect to the luminosity of the same star measured in another location of the CCD.

Using the measured star positions and fluxes, we performed a similar correction to that described by Bellini et al. (2009a). The correction is a self-consistent, autocalibration of the illumination map and takes advantage of the fact that the images are well dithered.

For each cluster and for each filter, the best image (characterized by lower airmass and best seeing) is defined as reference frame. We considered the measured raw magnitude m_{ij} of each star i in each image j. Using common stars between the image j and the reference frame we computed the average magnitude shift

$$\Delta_j = \frac{1}{M} \sum_{i=1}^{M} (m_{ij} - m_{i,\mathrm{ref}})$$

where M is the number of stars in common between the reference frame and the single image j. For each star that is centered

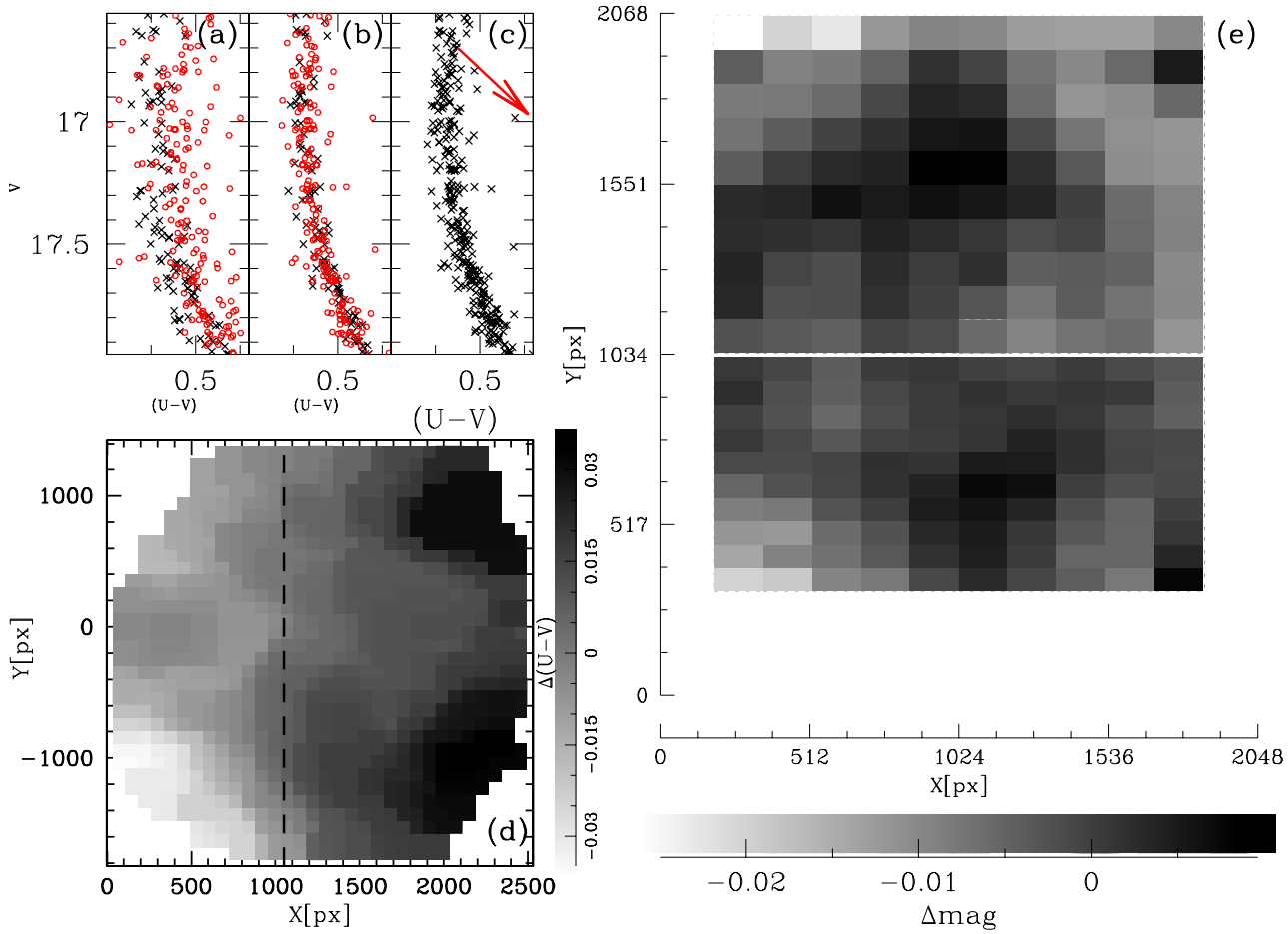

Fig. 3. Visualization of the effects of the photometric zero-point variation. Panel **a)**: CMDs zoomed into the MS region of NGC 6397 before the zero-point correction; panel **b)**: CMD after the zero-point correction; panel **c)**: CMD after the differential reddening correction (in red the reddening vector, scaled by a factor 1/3); panel **d)** map of the color zero-point variation; the dashed line divide the two groups of stars shown in the panels **a)** and **b)**; panel **e)**: final Δmag correction grid for the filter v_HIGH and the NGC 6397 data set.

in a different pixel in each dithered frame, we computed its average magnitude in the reference system

$$\bar{m} = \frac{1}{N}\sum_{j=1}^{N}(m_{ij} - \Delta_j)$$

where N is the number of images in which the star appears. Then we computed the residual:

$$\delta_{ij} = m_{ij} - \Delta_j - \bar{m}_j.$$

We divided each FORS2 chip in a spatial grid of 10×10 boxes, and, for each box, we computed the average of the residuals from the stars located in that region in each single image. This provides a first spatial correction to our photometry. To obtain the best correction, we iterate until the residual average becomes smaller than 1 mmag. To guarantee convergence, we applied half of the correction calculated in each box for each star. Moreover, to obtain the best correction at any location of the camera, we computed a bilinear interpolation of the closest four grid points. At the edges of the detectors the correction is less efficient because the corresponding grid points have been moved toward the external borders of the grid to allow the bilinear interpolation to be computed all across the CCDs. In panel (e) of Fig. 3, we show our final correction grid for the v_HIGH filter.

The final correction grids are different for each filter and for each set of images. In particular as well as the size of the zero-point variations, the patterns are different from filter to filter.

Table 2. Maximum amplitudes of photometric zero-point corrections.

Filter	Δmag		
	NGC 6121	NGC 6397	NGC 6752
u_HIGH	0.11	0.13	0.09
b_HIGH	0.04	0.05	0.03
v_HIGH	0.12	0.04	0.06
I_BESS	0.04	0.04	0.04

This quantity also changes using different data sets. The maximum amplitudes of our corrections are tabulated in Table 2.

We corrected the spread of the CMD due to differential reddening using the procedure as described by Milone et al. (2012b). Briefly, we defined a fiducial line for the MS of the cluster. Then, for each star, we considered a set of neighbors (usually 30, selected anew for each filter combination) and estimated the median offset relative to the fiducial sequence. These systematic color and magnitude offsets, measured along the reddening line, represent an estimate of the local differential reddening. With this procedure, we also mitigated the photometric zero-point residuals left by the illumination correction (especially close to the corners of the field of view). Panel (c) of Fig. 3 shows the CMD after all the corrections are applied.

The photometric calibration of FORS2 data for UBV Johnson and I_C Cousins bands was obtained using the

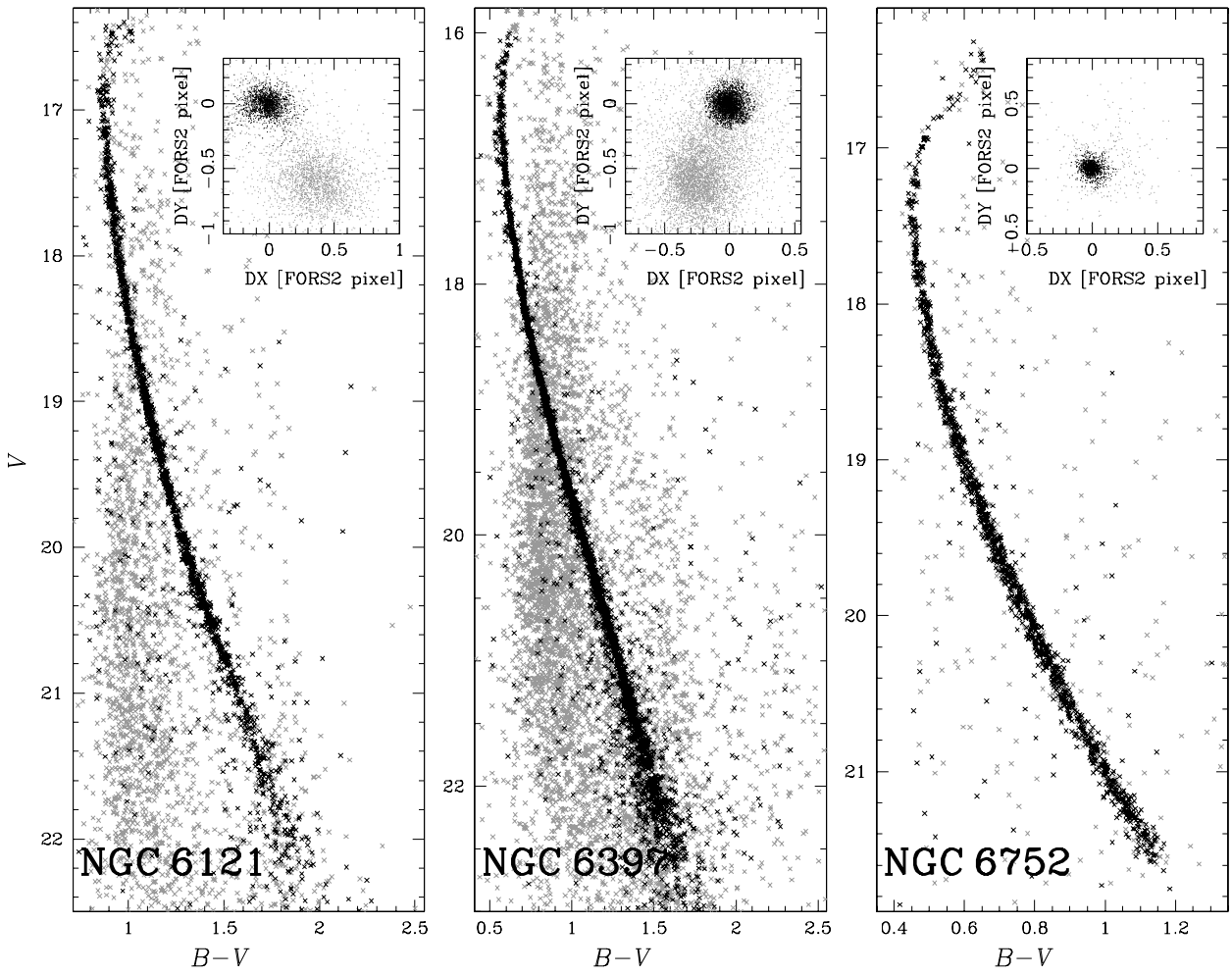

Fig. 4. The V versus $B-V$ CMD of stars in the field of view of NGC 6121 (*left*), NGC 6397 (*middle*), and NGC 6752 (*right*). The insets show the vector-point diagram of stellar displacements along the X and Y direction. Black and gray points indicate stars that, according to their proper motions, are considered cluster members and field stars, respectively (see text for details).

photometric Secondary Standards star catalog by Stetson (2000). We matched our final catalogs to the Stetson standard stars, and derived calibration equations by means of least squares fitting of straight lines using magnitudes and colors.

3.1. Proper motions

Since NGC 6121 (l, b = 350.°97, 15.°97) and NGC 6397 (l, b = 338.°17; −11.°96) are projected at low Galactic latitude, their CMDs are both dramatically contaminated by disk and bulge stars, in contrast to NGC 6752 (l, b = 336.°49; −25.°63) which presents low-field contamination. The average proper motions of NGC 6121, NGC 6397 and NGC 6752 strongly differ from those of these field stars (e.g., Bedin et al. 2003; Milone et al. 2006). Therefore, to minimize the contamination from field stars, we identified cluster members on the basis of stellar proper motions.

In order to get information on the cluster membership, we estimated the displacement between the stellar positions obtained from our FORS2 data set and those in the ground-based data taken from the image archive maintained by Stetson (2000) and also used in Monelli et al. (2013). These observations include images from different observing runs with the Max Planck 2.2 m telescope, the CTIO 4 m, 1.5 m and 0.9 m telescopes, and the Dutch 0.9 m telescope on La Silla. To obtain the displacement, we used six-parameter local transformations based on a sample of likely cluster members in close analogy to what was done by Bedin et al. (2003) and Anderson et al. (2006) to calculate stellar proper motions.

The results are shown in Fig. 4. The figure shows the V versus $B-V$ CMDs for NGC 6121, NGC 6397, and NGC 6752. The insets show the vector-point diagrams of the stellar displacements for the same stars shown in the CMDs: the cluster-field separation is evident. Likely cluster members are plotted in black both in the CMDs and in the vector-point diagrams, and in gray the rejected stars.

4. The CMDs of the three GCs

Previous studies on multiple stellar populations have demonstrated that the $U-B$ color is very efficient in detecting multiple RGBs (see Marino et al. 2008 and Milone et al. 2010 for the cases of NGC 6121 and NGC 6752), and multiple MSs (see Milone et al. 2012b, Mi13 for the cases of NGC 6397 and NGC 6752). As discussed by Sbordone et al. (2011), CNO abundance variations affect wavelengths shorter than ∼400 nm, owing to the rise of molecular absorption bands in cooler atmospheres. The consequences are that the CMDs in UB filters show enlarged sequences, mainly because of variations in the N abundance, with the largest variations affecting the RGB and the lower MS.

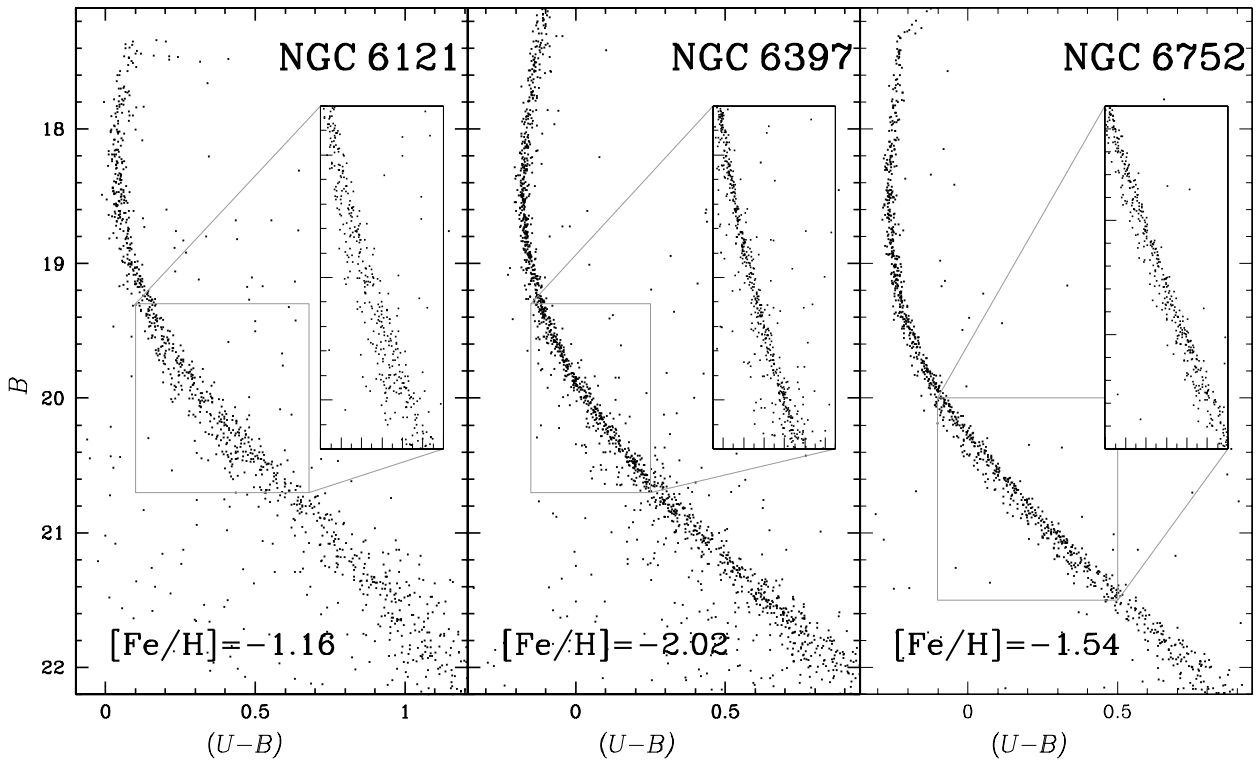

Fig. 5. The B versus $(U - B)$ CMD for NGC 6121 (*left*), NGC 6397 (*middle*), and NGC 6752 (*right*). The inset is a zoom around the upper MS. The CMDs only show the cluster members and are corrected by zero-point variations and differential reddening

Motivated by these results, we started our analysis from the B versus $U - B$ CMDs shown in Fig. 5; the inset of each panel is a zoom-in of the upper MS between ∼1.5 and ∼2.5 mag below the turn off (TO).

A visual inspection at these CMDs reveals that the color broadening of MS stars in both NGC 6121 and NGC 6752 is larger than that of NGC 6397. A small fraction of MS stars in NGC 6121 and NGC 6752 defines an additional sequence on the blue side of the most populous MS.

To investigate whether the widening of the MSs is due to the presence of multiple populations, we identified in the B versus $U - B$ CMD of each cluster two groups of red-MS (rMS) and blue-MS (bMS) stars, as shown in panels (a) of Fig. 6. We colored the two MSs in red and blue, respectively, and these colors are used consistently hereafter. In the case of NGC 6121 and NGC 6752, where there is some hint of a split MS, we identified by eye the fiducial that divide the rMS and bMS. In the case of NGC 6397, we have considered rMS (or bMS) as the stars that are redder (or bluer) than the MS fiducial line. Each inset shows the color distribution of $\Delta(U - B)$ for the two MSs, where $\Delta(U - B)$ is obtained by subtracting the color of the fiducial that divide the two MSs to the color of the rMS and bMS stars. In the cases of NGC 6121 and NGC 6752, the color distributions show a double peak that could be due to the presence of two populations; we fitted them with a sum of Gaussians (in red and blue for the rMS and bMS, respectively). We applied a moving box procedure to further verify that the distribution of $\Delta(U - B)$ in the case of NGC 6121 is bimodal. We changed the bin size, ranging from 0.005 to 0.02 (approximately the error in color) with steps of 0.001. Furthermore, from our data set we determined a kernel-density distribution by assuming a Gaussian kernel with $\sigma = 0.02$ mag. In all cases, we consistently found that the distribution can only be reproduced by two Gaussians.

A multiple sequence in NGC 6752 had already been identified by Mi13 using HST data. Very recently, we had the first *F275W*, *F336W*, *F438W WFC3* images of NGC 6121 from the HST GO-13297 UV large legacy program (P.I. Piotto). Even a preliminary reduction of the data shows a clear separation of the MS into two branches in the *F438W* vs. *F336W–F438W* CMD, fully confirming what we anticipate here in the equivalent, groundbased U vs. $U - B$ diagram of Fig. 6. In the case of NGC 6397, it is possible to fit the distribution with a single Gaussian.

As an additional check for the presence of multiple populations, we investigated whether the widening of the MSs of all the GCs is intrinsic or if it is entirely due to photometric errors. We have compared two CMDs, B versus $U - B$ with V versus $V - I$, obtained using independent data sets. We considered the rMS and bMS defined previously: if the color spread is entirely due to photometric errors, a star that is red (or blue) in the B versus $U - B$ CMD will have the same chance of being either red or blue in the V vs. $V - I$ CMD. By contrast, the fact that the two sequences identified in the first CMD have systematically different colors in the second CMD would be a proof that the color broadening of the MS is intrinsic. In panels (b) of Fig. 6 we plotted the rMS and bMS in V versus $V - I$ CMDs. The fact that the rMS stars of both NGC 6121 and NGC 6752 have, on average, different $V - I$ than bMS stars demonstrates that the color broadening of their MS in the U versus $U - B$ CMDs is intrinsic. This is the first evidence that the MS of NGC 6121 is not consistent with a simple stellar population. In the case of NGC 6397, rMS and bMS stars share almost the same $V - I$ thus suggesting that most of the colors broadening is due to photometric errors.

As a last test, we plotted the two MSs in the V versus $c_{U,B,I}$ CMD. The $c_{U,B,I}$ index, which is defined as the color difference $(U - B) - (B - I)$, is a very efficient tool to identify multiple

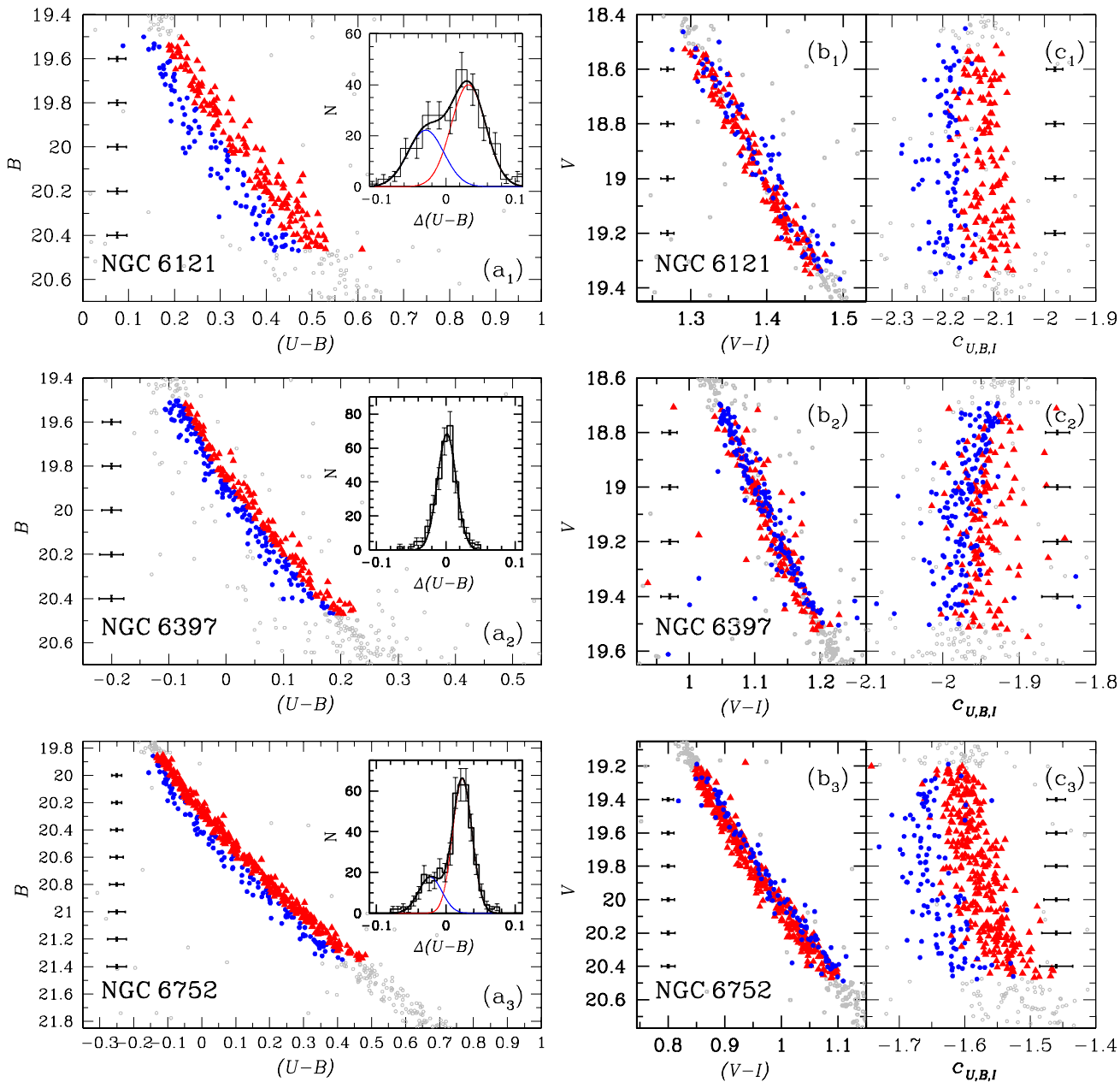

Fig. 6. Comparison between the B vs. $U-B$ (panels **a**)), the V vs. $V-I$ (panels **b**)) and V vs. $c_{U,B,I}$ (panels **c**)) CMDs of NGC 6121 (*up*), NGC 6397 (*middle*) and NGC 6752 (*down*). Red triangles and blue points represent the groups of rMS and bMS stars defined in panels **a**). The insets of panels **a)** show the $\Delta(U-B)$ distributions, fitted with a bigaussian in the case of NGC 6121 and NGC 6752 and with a Gaussian in the case of NGC 6397. The horizontal bars show the mean error in color.

sequences in GCs. Indeed, it maximizes the color separation between the stellar populations that is due to both helium and light-element variations (Monelli et al. 2013). Panels (c) of Fig. 6 confirm the previous results: rMS and bMS of NGC 6121 and NGC 6752 are well defined in the V versus $c_{U,B,I}$ CMDs, but this is less evident for NGC 6397.

As a last proof, we plotted in Fig. 7 the $(U-B)$ versus $(V-I)$ diagrams for each cluster: the rMS and bMS are plotted in red and blue as defined previously. The figure shows that for both NGC 6121 and NGC 6752 the two MSs are well defined, while for NGC 6397 the rMS and bMS stars are mixed.

Figure 8 shows the V versus $c_{U,B,I}$ diagram for the three GCs under study here. In their analysis of multiple stellar populations in 22 GCs, Monelli et al. (2013) found that all the analyzed clusters show a multimodal or spread RGB in the V versus $c_{U,B,I}$ diagram, and the $c_{U,B,I}$ value of each star depends on its light-element abundance. The $c_{U,B,I}$-index width of the RGB ($W_{\rm RGB}$) correlates with the cluster metallicity, with the more metal rich GCs also having the largest values of $W_{\rm RGB}$. In order to compare the MSs of the three GCs we studied, we introduce a quantity, $W_{\rm MS}$, which is akin to $W_{\rm RGB}$, but is indicative of the $c_{U,B,I}$-index broadening of the MS. The procedure to determine $W_{\rm MS}$ is illustrated in Fig. 9 for NGC 6121 and is the same for the other clusters. We have considered the magnitude of the TOs as magnitude of reference: $V_{\rm MSTO} \sim 16.6$ in the case of NGC 6397, $V_{\rm MSTO} \sim 17.4$ for NGC 6752, and $V_{\rm MSTO} \sim 16.75$ for NGC 6121. Panel (a) of Fig. 9 shows the V versus $c_{U,B,I}$ diagram for NGC 6121 in a range of magnitudes from $V_{\rm MSTO} - 0.5$ to $V_{\rm MSTO} + 5$. In this range of magnitudes, we obtained the fiducial line for the MSs computing the 3.5σ-clipped median

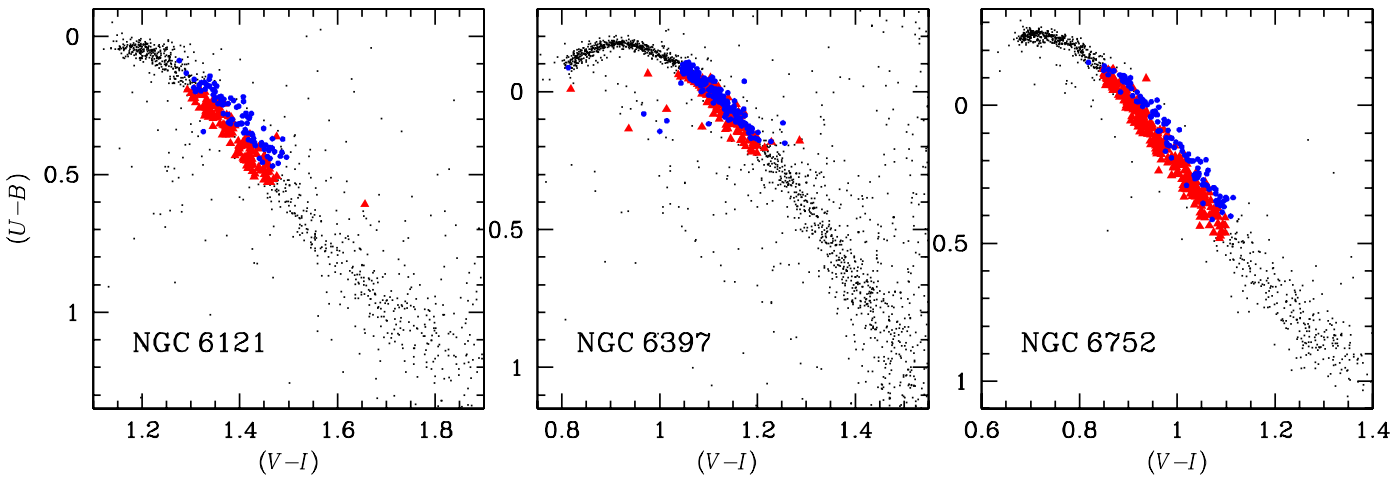

Fig. 7. Color–color diagrams for NGC 6121 (*left panel*), NGC 6397 (*central panel*), and NGC 6752 (*right panel*). In red (triangles) and blue (dots) we show the rMS and bMS as defined in Fig. 6

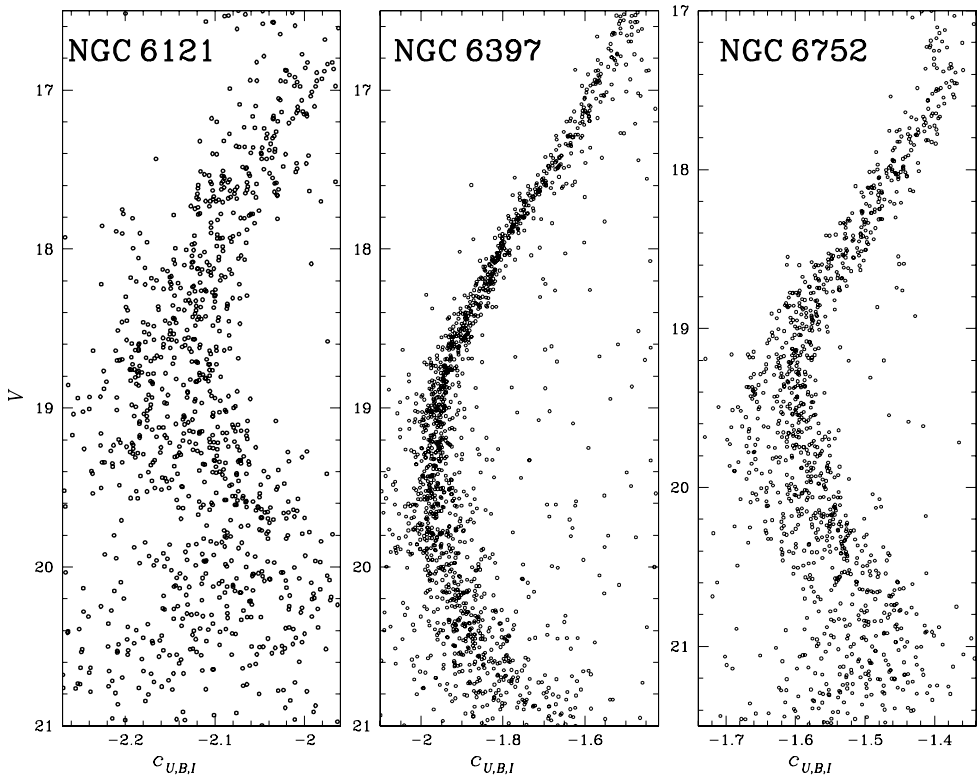

Fig. 8. V, $c_{U,B,I}$ diagrams for NGC 6121 (*left*), NGC 6397 (*middle*), and NGC 6752 (*right*).

of the color in the interval of 0.35 mag and interpolated these points with a spline. In our analysis, we only used MS stars with $2 < V - V_{\rm MSTO} < 2.5$, where the MS split is visible for both NGC 6121 and NGC 6752. This magnitude interval is delimited by the two dashed lines of Fig. 9a. The thick line is the fiducial in the considered magnitude interval. The verticalized V versus $\Delta c_{U,B,I}$ diagrams is plotted in panel (b) of Fig. 9, while panel (c) shows the histogram distribution of $\Delta c_{U,B,I}$. The MS width, $W_{\rm MS}$, is defined as the $\Delta c_{U,B,I}$ extension of the histogram and is obtained by rejecting the 5% of the reddest and the bluest stars on the extreme sides. To account for photometric error, we have subtracted from the observed $W_{\rm MS,OBS}$ the average error in $c_{U,B,I}$ in the same magnitude interval, i.e., $W_{\rm MS} = \sqrt{W^2_{\rm MS,OBS} - \sigma^2_{c_{U,B,I}}}$. We found that the most metal-rich GC, NGC 6121, exhibits the largest $c_{U,B,I}$ index width for MS stars ($W_{\rm MS} = 0.169 \pm 0.014$). The spread in $c_{U,B,I}$ is smaller in the case of NGC 6752 ($W_{\rm MS} = 0.115 \pm 0.006$) and drops down to $W_{\rm MS} = 0.093 \pm 0.014$ in the most metal-poor GC NGC 6397. To estimate the statistical uncertainty in measuring $W_{\rm MS}$, we used the bootstrap resampling of the data to generate 10 000 samples drawn from the original data sets. We computed the standard deviation from the mean of the simulated $W_{\rm MS}$ and adopted this as the uncertainty of the observed $W_{\rm MS}$.

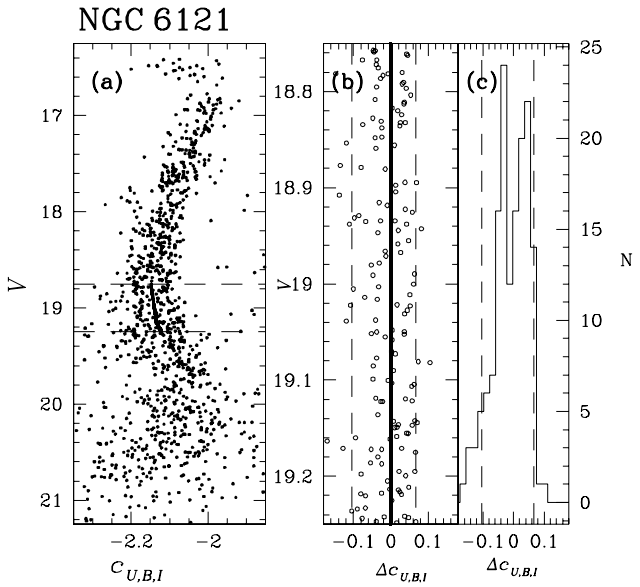

Fig. 9. Procedure to estimate the MS width for NGC 6121. Panel **a)** shows the V versus $c_{U,B,I}$ CMD of NGC 6121. The thick line is the MS fiducial line (see text for details). Panel **b)** shows the verticalized MS between the two dashed lines of panel **a)**. Panel **c)** is the distribution of the color for the stars of panel **b)**.

These findings make it tempting to speculate that the $c_{U,B,I}$ index width of the MS could be correlated with the cluster metallicity in close analogy with what we observed for RGB stars. An analysis of a large sample of GCs is mandatory to infer any conclusion on the relation between $W_{\rm MS}$ and [Fe/H].

Milone et al. (2013) have identified three stellar populations in NGC 6752 that they have named "a", "b", and "c". Population "a" has a chemical composition similar to field halo stars of the same metallicity, population "c" is enhanced in sodium and nitrogen, depleted in carbon and oxygen and enhanced in helium ($\Delta Y \sim 0.03$), while population "b" has an intermediate chemical composition between "a" and "c" and is slightly helium enhanced ($\Delta Y \sim 0.01$). However, the MSs of populations "b" and "c" are nearly coincident in the m_{F336W} versus $m_{F336W} - m_{F390W}$ CMD, while population "a" stars have bluer $m_{F336W} - m_{F390W}$ colors (Mi13, see their Fig. 8). The three MSs also exhibit a similar behavior in the $m_{F336W} - m_{F410M}$ and $m_{F336W} - m_{F467M}$ colors. Since these colors are similar to $U - B$, the less populous MS identified in this paper should correspond to the population "a" identified by Mi13, while the rMS hosts both population "b" and population "c" stars.

4.1. The fraction of rMS and bMS in NGC 6121 and NGC 6752

In order to measure the fraction of stars in each MS, we followed the procedure illustrated in Fig. 10 for NGC 6752, which we already used in several previous papers (e.g., Piotto et al. 2007; Mi13).

Panel (a) shows the V versus $c_{U,B,I}$ CMD of the MS stars in the magnitude interval $19.25 < V < 20.55$, where the MS split is most evident. We verticalized the selected MS by subtracting the color of the stars to the color of the fiducial line of the rMS, obtaining $\Delta c_{U,B,I}$. The fiducial line is obtained by hand selecting the stars of the rMS, dividing them in bins of magnitude, computing the median colors of the stars within each bin, and interpolating these median points with a spline. The verticalized V versus $\Delta c_{U,B,I}$ diagram is plotted in panel (b).

The $\Delta c_{U,B,I}$ color distribution of the stars for three magnitude intervals is shown in panels (c). Each histogram clearly shows two peaks and has been simultaneously fitted with a double Gaussian, whose single components are shown in blue and red for the bMS and the rMS, respectively.

For each magnitude interval, we infer the fraction of bMS and rMS stars from the area under the Gaussians. The errors (σ) associated with the fraction of stars are estimated as $\sigma = \sqrt{\sigma_{\rm I}^2 + \sigma_{\rm II}^2}$, where $\sigma_{\rm I}$ is derived from binomial statistics and $\sigma_{\rm II}$ is the uncertainty introduced by the histogram binning and is derived as in Libralato et al. (2014). Briefly, we have derived N times the population ratio as described above, but by varying the binning and starting/ending point in the histogram. We assumed $\sigma_{\rm II}$ as the rms scatter of these N determinations.

We computed the weighted mean of the bMS and rMS fractions of the three magnitude intervals, using as weight $w = 1/\sigma^2$. In the case of V versus $c_{U,B,I}$, we obtained that the rMS and bMS contain 75% ± 3% and 25% ± 5% of MS stars, respectively. In panels (d)–(f) of Fig. 10, we applied the same procedure in the B versus $(U - B)$ using the stars with $20.10 < B < 21.45$. We found that the blue MS contains 27% ± 5% of the total number of MS stars, and the red MS is made of the remaining 73% ± 3% stars. We also calculated the weighted mean of the results of the two CMDs of NGC 6752, finding that there are the 74% ± 2% of stars in the rMS, and the remaining 26% ± 4% are in the bMS.

We have already demonstrated that the $\Delta(U - B)$ distribution, in the B versus $U - B$ CMD of NGC 6121, shows a double peak, proving the presence of multiple populations (see panel a_1 of Fig. 6). We performed a detailed analysis of the MS of NGC 6121, applying the same procedure described for NGC 6752. The procedure and the results are shown in Fig. 11. We find from the analysis of the B versus $U - B$ CMD that the bMS contains 31% ± 8% of MS stars, and the rMS includes the remaining 69% ± 7%. In the case of the V versus $c_{U,B,I}$ diagram, we infer that rMS and bMS contain 61% ± 4% and 39% ± 5% of the total number of MS stars, respectively. We computed the fraction of rMS and bMS for NGC 6121 using different histogram bin sizes and changing starting/ending points. We used bin sizes with values between 0.005 and 0.025 (larger than color error), starting points between −0.5 and −0.15 and ending points between 0.15 and 0.5. In all cases, the resulting fraction of stars are in agreement with the values we quote above within the errors. The results from the two CMDs imply that in the rMS and bMS there are 63% ± 3 % and 37% ± 4% of MS stars, respectively.

5. The radial distribution of stellar populations in NGC 6752 and NGC 6121

The analysis of the radial distribution of rMS and bMS stars in NGC 6121 and NGC 6752 is an important ingredient to shed light on the formation and the evolution of multiple stellar populations in these GCs. Indeed, theoretical models predict that, when the GC forms second-generation stars should be more centrally concentrated than first-generation stars, and many GCs could still keep memory of the primordial radial distribution of their stellar populations (e.g., D'Ercole et al. 2008; Bekki 2011; Vesperini et al. 2013).

The radial distribution of stellar populations in NGC 6752 is still controversial. Kravtsov et al. (2011) determined wide field, multiband photometry of NGC 6752 and studied the distribution

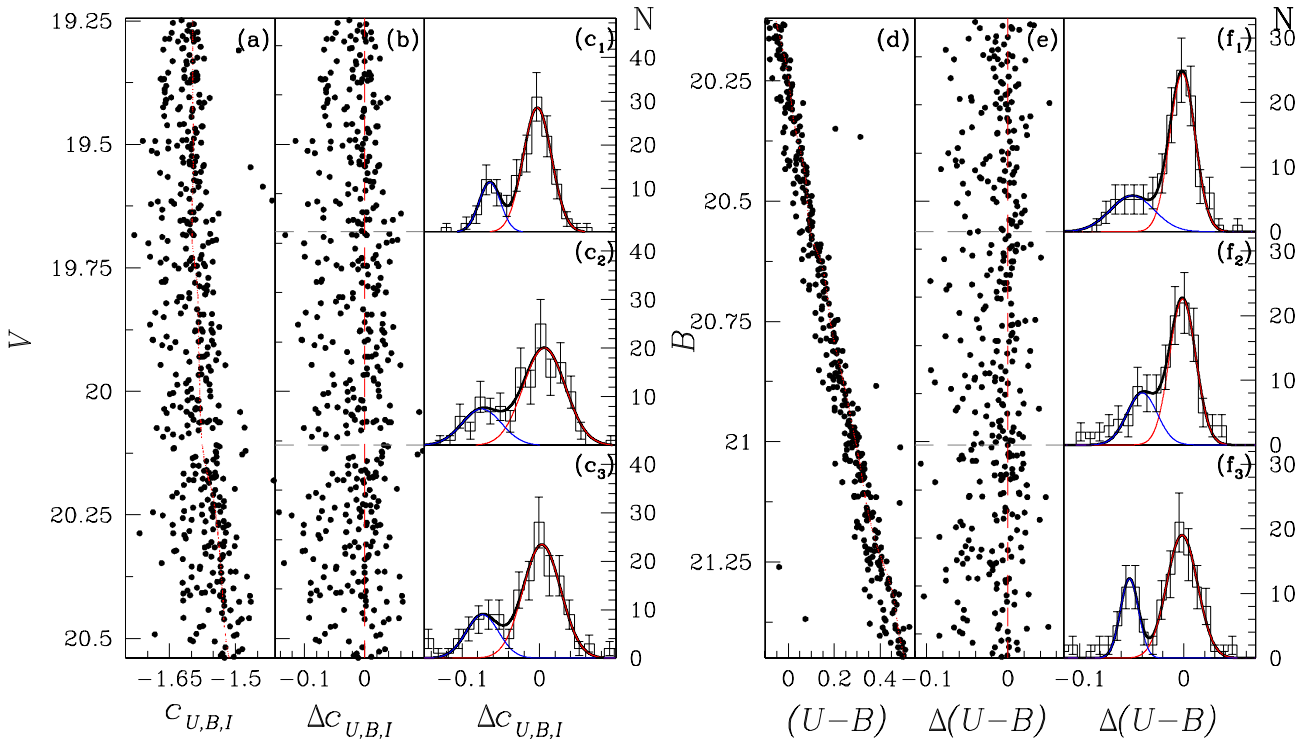

Fig. 10. Procedure to estimate the fraction of rMS and bMS stars in NGC 6752 using the V versus $c_{U,B,I}$ diagram (panels **a)**, **b)**, and **c)**), and the B versus $U - B$ CMD (panels **d)**, **e)**, and **f)**). Panels **a)** and **d)** reproduce the same diagrams as Figs. 8 and 5. The red line is the rMS fiducial line. Panels **b)** and **e)** show the verticalized MS. The histogram distribution of Δ(color) for the stars of the panel **b)** and **e)** is plotted in panels **c)** and **f)** for three intervals of magnitude. The thick black lines, superimposed to each histogram, are the best-fitting biGaussian functions, whose components are colored red and blue. In the case of V versus $c_{U,B,I}$ CMD, we found that rMS and bMS contain 77 ± 4% and 23 ± 8% of MS stars in panel **c1)**, 74 ± 5% and 26 ± 8% of MS stars in panel **c2)** and, 75 ± 5% and 25 ± 8% of the MS stars, respectively. In the case of B versus $(U - B)$ CMD, we found that rMS and bMS contain 72 ± 5% and 28 ± 8% of MS stars in panel **f1)**, 74 ± 6% and 26 ± 9% of MS stars in panel **f2)**, 73 ± 5% and 27 ± 8% of MS stars in panel **f3)**, respectively.

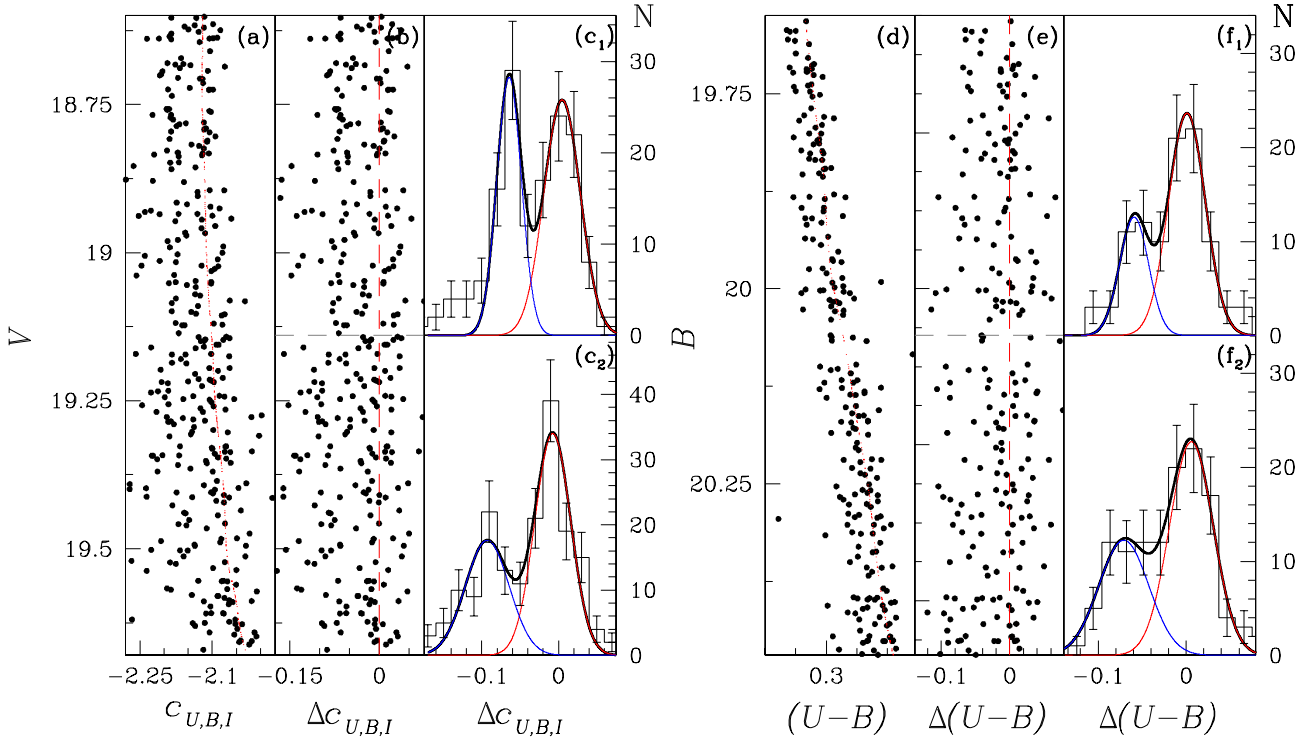

Fig. 11. As in Fig. 10, in the case of NGC 6121. In the case of V versus $c_{U,B,I}$ CMD, we found that rMS and bMS contain 60 ± 7% and 40 ± 8% of MS stars in panel **c1)**, 61 ± 6% and 39 ± 7% of MS stars in panel **c2)**, respectively. In the case of B versus $(U - B)$ CMD, we found that rMS and bMS contain 67 ± 7% and 33 ± 10% of MS stars in panel **f1)**, 75 ± 13% and 25 ± 14% of MS stars in panel **f2)**, respectively.

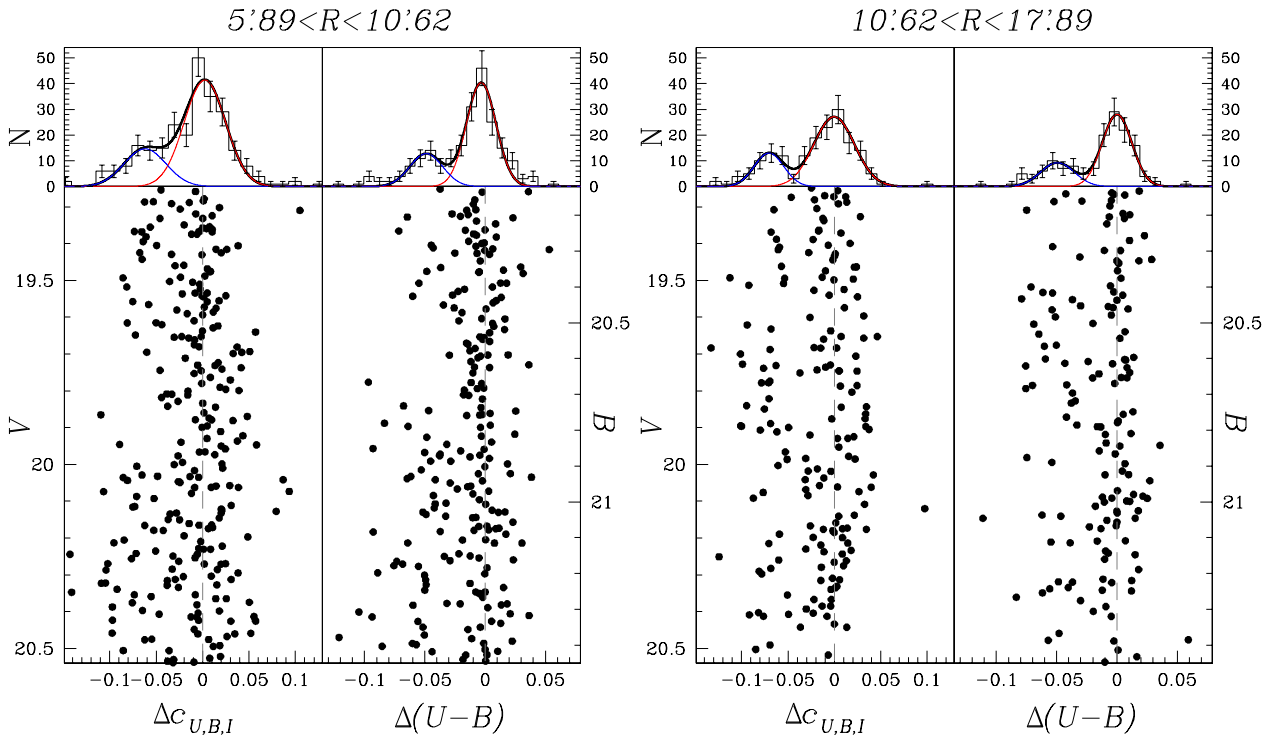

Fig. 12. Color distribution analysis for the MSs stars of NGC 6752 in two different radial bin, containing almost the same number (855 and 854) of stars. In the inner field (*left panels*) we found that MSa (blue) and MSbc (red) contain 28 ± 6% and 72 ± 4% of MS stars, respectively, in the V versus $c_{U,B,I}$ CMD, and 27 ± 6% and 73 ± 4% of MS stars, respectively, in the B versus $(U - B)$ CMD. In the outer field (*right panels*) we found that MSa and MSbc contain 26 ± 7% and 74 ± 4% of MS stars, respectively, in the V versus $c_{U,B,I}$ CMD, and 29 ± 8% and 71 ± 6% of MS stars, respectively, in the B versus $(U - B)$ CMD.

of its stellar populations across the field of view. They concluded that there is a strong difference in the radial distribution between the populations of RGB stars that are bluer (bRGB) and redder (rRGB) in $(U - B)$ color, and obtained similar findings from the study of the SGB. Specifically, at a radial distance close to the half-mass radius (r_h = 1′.91; Harris 1996, 2010 edition) the fraction of rRGB stars abruptly decreases. These results are in disagreement with the conclusions by Mi13 who showed that the three stellar populations identified in their paper share almost the same radial distribution. Kravtsov and collaborators analyzed stars with a radial distance from the center of NGC 6752 out to ∼9′.5, while the study by Mi13 is limited to the innermost ∼6 arcmin. We extend our analysis to larger radii[1].

As already mentioned in Sect. 4, we suggest that the bMS of NGC 6752 corresponds to the population "a" identified by Mi13, while the most populous rMS hosts both population "b" and population "c" stars of Mi13. For this reason, in this section we rename the bMS in MSa and the rMS in MSbc.

To investigate the radial distribution of stellar populations within the field of view analyzed in this paper, we divided the catalog of NGC 6752 stars into two groups at different radial distance from the cluster center, each containing almost the same total number of stars.

The inner sample of stars (inner field) lies between 5′.89 and 10′.62 from the cluster center. The outer group of stars (outer field) is between 10′.62 and 17′.89 from the center. We estimated the fraction of stars in each group, following the same procedure described in Sect. 4.1.

The results are illustrated in Fig. 12. In the left panels, we show the verticalized V versus $\Delta c_{U,B,I}$ and the B versus $\Delta(U - B)$ diagrams for stars in the inner field. In this region, the MSa contains 27% ± 4% and the MSbc hosts the remaining 73% ± 3% of the total number of MS stars. In the outer field (right panels of Fig. 12), the MSa and the MSbc are made of the 27% ± 5% and 73% ± 3% of MS stars, respectively. We conclude that there is no evidence for a gradient within the field of view studied in this paper.

To further investigate the radial distribution of stellar populations in NGC 6752 we compare our results for stars with a distance from the cluster center larger than ∼6 arcmin and the fraction of stars that have been estimated by Mi13 in the internal regions using the same method.

Since the MSbc contains both populations "b" and population "c" stars, we have added together the fractions of population "b" (f_{POPb}) and population "c" stars (f_{POPc}) listed by Milone et al. (2013, see their Table 4) and calculated the fraction of stars in these two populations: $f_{POPbc} = f_{POPb} + f_{POPc}$. As aforementioned in Sect. 4, we further compare the fractions of population "a" stars by Mi13, with the fractions of MSa stars derived in this paper. The values of f_{POPa} and f_{POPbc} are listed in Table 3.

Results are shown in Fig. 13, where the top panels show the distribution of the fraction of population "a" (in blue) and the fraction of population "b"+"c" (in red) as a function of the radial distance from the cluster center, while the bottom panels show the radial trend of the ratio between the fraction of population "a" and the fraction of population "b"+"c". In the left panels, we show both the above described distributions considering single radial intervals for each set of data, while in the right

[1] We assume that stars in the fields of NGC 6752 and NGC 6121 are representative of stellar populations at the studied radial distance; we are not able to investigate any dependency on the angular position using the data set presented in this work.

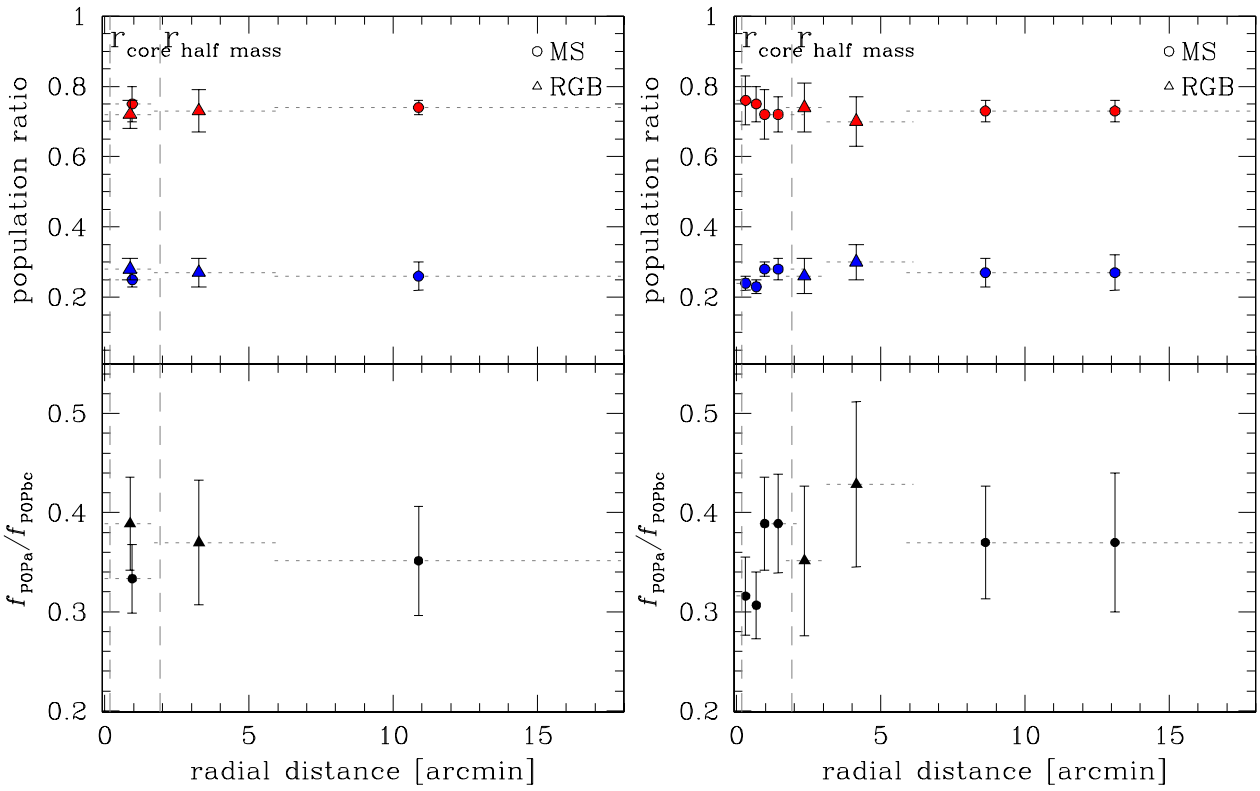

Fig. 13. *Top*: radial distribution of the fraction of population "a" (blue) and "b"+"c" (red) stars with respect the total number of stars. *Bottom*: radial trend of the ratio between f_{POPa} and f_{POPbc} stars. At *left*, we consider single radial interval for each set of data, while in the *right* panel we divide the radial interval in different bins. The distribution seems to be flat in both cases.

Table 3. Fraction of POPa and POPbc stars for NGC 6752.

R_{min}	R_{max}	R_{ave}	f_{POPa}	f_{POPbc}	Seq.
0.00	1.70	0.95	0.25 ± 0.02	0.75 ± 0.05	MS
0.00	1.70	0.87	0.28 ± 0.03	0.72 ± 0.04	RGB
1.70	6.13	3.26	0.27 ± 0.04	0.73 ± 0.06	RGB
5.89	17.89	10.88	0.26 ± 0.04	0.74 ± 0.02	MS
0.00	0.53	0.31	0.24 ± 0.02	0.76 ± 0.07	MS
0.53	0.83	0.68	0.23 ± 0.02	0.75 ± 0.05	MS
0.83	1.12	0.97	0.28 ± 0.02	0.72 ± 0.07	MS
1.12	2.33	1.44	0.28 ± 0.03	0.72 ± 0.05	MS
1.70	3.11	2.35	0.26 ± 0.05	0.74 ± 0.07	RGB
3.11	6.13	4.15	0.30 ± 0.05	0.70 ± 0.07	RGB
5.89	10.62	8.63	0.27 ± 0.04	0.73 ± 0.03	MS
10.62	17.89	13.12	0.27 ± 0.05	0.73 ± 0.03	MS

panels we divided each radial interval into different bins. Our findings suggest that there is no evidence for a radial gradient among population "a" and population "b"+"c" of NGC 6752.

To investigate the radial distribution of stellar populations in NGC 6121, we divided the field of view we analyzed into two regions, with a radial distance from the cluster center of $5\farcm12 < R < 9\farcm63$ (inner field) and $9\farcm63 < R < 17\farcm81$ (outer field). Each region contains almost the same number of stars. We determined the fraction of rMS and bMS stars by following the same recipe described in detail for NGC 6752. The results are shown in Fig. 14. We found that in the inner field the fraction of bMS is 40% ± 13% and the fraction of rMS is 60% ± 13%. For the outer field we find that the bMS and the rMS contains 36% ± 6% and 64% ± 4% of the total number of the considered MS, respectively. Also for NGC 6121, we found no evidence of population gradients.

6. The helium content of stellar populations in NGC 6121 and NGC 6752

The ultraviolet passband is very efficient at separating multiple sequences due to its sensitivity to difference in C, N, O abundance (Marino et al. 2008; Sbordone et al. 2011). In contrast, $B-I$ and $V-I$ colors are marginally affected by light-element variations, but are very sensitive to the helium abundance of the stellar populations (e.g., D'Antona et al. 2002; Piotto et al. 2007; Sbordone et al. 2011; King et al. 2012; Cassisi et al. 2013), thus providing us with an efficient tool to infer the helium content.

6.1. NGC 6121

The procedure to estimate the average helium difference between bMS and rMS stars for NGC 6121 is illustrated in Fig. 15 and is already used in several papers by our group (Mi13, Milone et al. 2012a,c). Since we have already extracted the stellar populations in NGC 6121 using the B versus $U-B$ CMD of Fig. 11, we can now follow them in any other CMD. By combining photometry in four filters, we can construct three CMDs with I versus $(X-I)$, where $X = U, B, V$. The fiducial lines of bMS and rMS in these CMDs are plotted in the upper panels of Fig. 15. The rMS fiducial line is redder than the bMS fiducial line in $U-I$ color, whereas the rMS fiducial lines are bluer in $B-I$ and $V-I$ colors.

We measured the $X-I$ color distance between the two MSs at a reference magnitude (I_{CUT}) and repeated this procedure for I_{CUT} = 17.3, 17.5, 17.7, 17.9, and 18.1 (corresponding to the magnitude interval where the two MS separations is maximal, cf. Fig. 6). The color difference $\Delta(X-I)$ is plotted in the lower

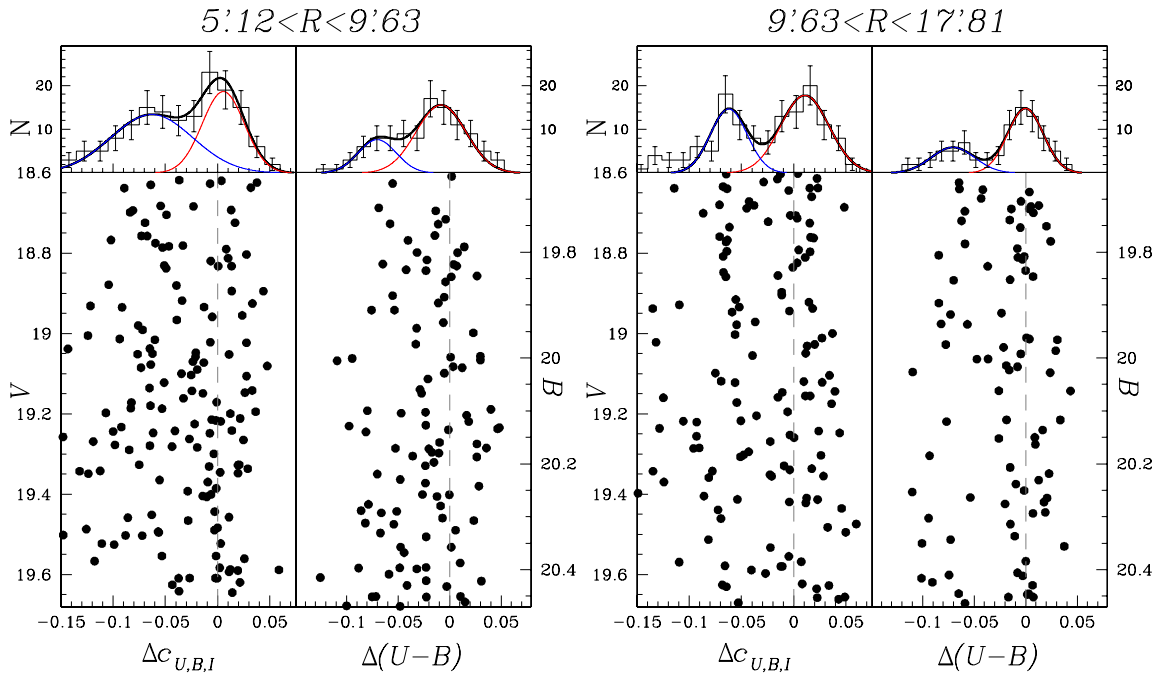

Fig. 14. Color distribution analysis for the MSs stars of NGC 6121 in two different radial bin, containing almost the same number (754 and 755) of stars. In the inner field (*left panels*) we found that rMS and bMS contain 42 ± 20% and 58 ± 20% of MS stars, respectively, in the V versus $c_{U,B,I}$ CMD, and 73 ± 16% and 27 ± 17% of MS stars, respectively, in the B versus $(U - B)$ CMD. In the outer field (*right panels*) we found that rMS and bMS contain 62 ± 6% and 38 ± 7% of MS stars, respectively, in the V versus $c_{U,B,I}$ CMD, and 67 ± 6% and 33 ± 9% of MS stars, respectively, in the B versus $(U - B)$ CMD.

panel of Fig. 15 as a function of the central wavelength of the X filter (gray dots), for the case of $I_{\rm CUT} = 17.7$.

We estimated effective temperatures ($T_{\rm eff}$) and gravities ($\log g$) at different $I = I_{\rm CUT}$ for the two MS stars and for the different helium contents using BaSTI isochrones (Pietrinferni et al. 2004, 2009).

We assumed a primordial helium abundance for the bMS, $Y = 0.248$, and used different helium content for the rMS, with Y varying from 0.248 to 0.400 with steps of $\Delta Y = 0.001$. To account for the appropriate chemical composition of the two stellar populations of NGC 6121, we assumed the abundances of C, N, O, Mg, Al, and Na for the bMS and the rMS as measured for first and second-generation RGB stars listed by Marino et al. (2008, see their Table 6).

We used the ATLAS12 program and the SYNTHE code (Kurucz 2005; Castelli 2005; Sbordone et al. 2007) to generate synthetic spectra for the adopted chemical compositions, from ∼2500 Å to ∼10 000 Å. Synthetic spectra have been integrated over the transmission curves of the U, B, V, I filters, and we calculated the color difference $X - I$ for each value of helium of our grid.

The best-fitting model is determined by means of chi-square minimization. Since the U magnitude is strongly affected by the abundance of light elements, we used $B - I$ and $V - I$ colors only to estimate Y. The helium difference corresponding to the best-fit models are listed in Table 4 for each value of $I_{\rm CUT}$.

We derived that the rMS is slightly helium enhanced with respect to the bMS (which has $Y = 0.248$), with an average helium abundance of $Y = 0.268 \pm 0.008$. This is the internal error estimated as the rms scatter of the $N = 5$ independent measurements divided by the square root of $N - 1$. Results are shown in Fig. 15, for the case of $I_{\rm CUT} = 17.7$, where we represented the synthetic colors corresponding to the best-fitting model as red asterisks.

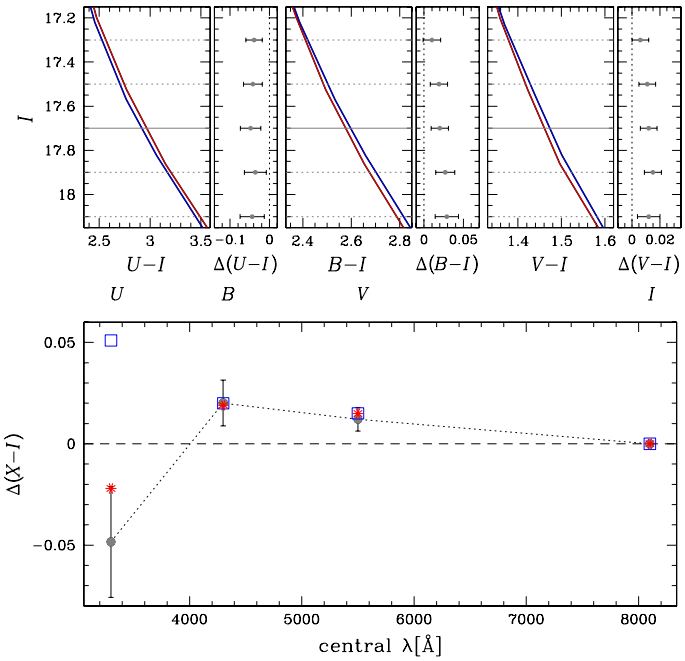

Fig. 15. *Top panels*: MS fiducial in 3 $X - I$ CMDs ($X = U, B, V$) of NGC 6121. The horizontal lines represent the magnitudes $I_{\rm CUT}$ for which the color distance between the two MSs is calculated. For each $I_{\rm CUT}$ the error in $\Delta(X - I)$ is shown. *Bottom panel*: $X - I$ color distance between rMS and bMS at $I_{\rm CUT} = 17.7$ as a function of the central wavelength of the X filter. Observations are represented with gray dots. Red asterisks are the best-fitting model, while blue squares are the results obtained calculating synthetic colors of two MS stars with the same light-element chemical composition, but different He content. The blue squares demonstrate that the abundance of light elements assumed in the model does not affect the results of the He abundance of the two MSs in the optical colors, but strongly affects the U band.

Table 4. Parameters used to simulate synthetic spectra of rMS and bMS stars and estimation of helium difference between the two population for different I_{CUT} in the case of NGC 6121.

I_{CUT}	$T_{EFF,bMS}$	$T_{EFF,rMS}$	$\log g_{bMS}$	$\log g_{rMS}$	ΔY
17.3	5542	5571	4.58	4.57	0.014
17.5	5397	5444	4.60	4.60	0.021
17.7	5247	5297	4.63	4.63	0.022
17.9	5095	5149	4.65	4.65	0.024
18.1	4944	4989	4.66	4.66	0.021
Average					0.020, $\sigma = 0.008$

For completeness, we also calculated synthetic colors of two MS stars with the $I = I_{CUT}$ and the same chemical composition (same abundance of light elements). We assumed for bMS primordial helium and for rMS the helium abundance of the best-fitting model. Results are represented as blue squares in Fig. 15 and confirm that the abundance of light elements assumed in the model does not affect our conclusion on the helium abundance of the two MSs, which are based on the optical colors. Instead, the different CNO content strongly affect the U band.

In principle, the He content of stellar populations in GCs can also be estimated using He lines in HB star spectra (e.g., the HeI line at $\lambda = 5875.6$ Å line, Villanova et al. 2009, 2012; Marino et al. 2014). However, spectroscopic measurement of He in GC stars has many limitations. First of all, He can only be measured for stars in a very limited temperature interval ($8500 < T < 11\,500$ K). In fact, stars with $T \leq 8500$ K are not sufficiently hot to form He lines, while stars bluer than the Grundahl jump (Grundahl et al. 1999, $T \geq 11\,500$ K) are affected by He sedimentation and metal levitation, which alter the original surface abundance. The HB of NGC 6121 is populated on both the red and the blue side of the RR Lyrae instability strip. Spectroscopic investigation by Marino et al. (2011) reveals that the blue HB is made of second population Na-rich and O-poor stars, while red HB stars belong to the first population. In NGC 6121, the HB segment with $8500 < T < 11\,500$ K corresponds to the blue HB, and therefore it only provides partial information only. In this cluster (as in many others), it is not possible to spectroscopically measure the He content of the first population.

Villanova et al. (2012) have used the HeI line at $\lambda = 5875.6$ to estimate the helium content of six blue-HB stars in the blue HB of NGC 6121. All of them are second-population stars. They derived a mean value of $Y = 0.29 \pm 0.01$ (random) ± 0.01 (systematic) and conclude that second-population stars would be enhanced in helium by $\sim$0.04–0.05 dex. This estimate of the He content has been made by assuming local thermodynamic equilibrium (LTE) approximation. However, the HeI line at $\lambda = 5875.6$ is affected by non-local thermodynamic equilibrium (NLTE) effect, which can cause an error in the Y estimate as large as $\Delta Y = 0.10$ (see Marino et al. 2014 for the case of NGC 2808). Appropriate NLTE analysis is required to infer reliable He abundances from spectroscopy of HB stars in NGC 6121. In contrast, the He difference between red- and blue-MS stars in NGC 6121 comes from the colors of the fiducial lines, which have small color uncertainties.

6.2. NGC 6752

We followed the same procedure to estimate the average helium difference between MSa and MSbc stars. We measured the color distance between the two fiducial lines of MSa and MSbc in the I versus $(X - I)$ CMDs (Fig. 16), where $X = U, B, V$, at reference magnitudes $I_{CUT} = 18.55$, 18.75, 18.95, 19.15 and 19.35. The color difference $\Delta(X - I)$ at $I_{cut} = 18.95$ is plotted in the bottom panel of Fig. 16 as a function of the central wavelength of the X filter.

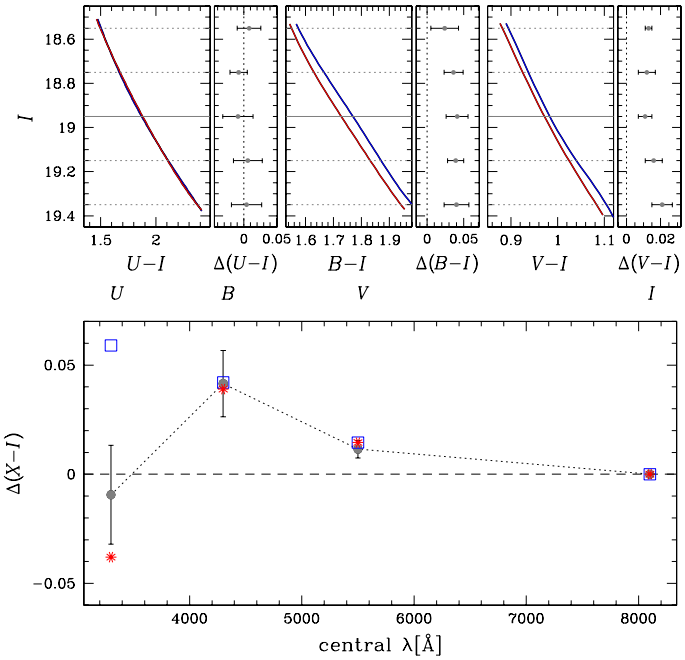

Fig. 16. As in Fig. 15, in the case of NGC 6752. In the *top panels*, the fiducial blue is that of the MSa and the red fiducial is for MSbc.

We used BaSTI isochrones (Pietrinferni et al. 2004, 2009) to estimate T_{eff} and $\log g$ at different I_{CUT}.

We assumed that MSa has primordial helium abundance, $Y = 0.248$, and varied the helium content of the MSbc between 0.248 and 0.400 in steps of $\Delta Y = 0.001$. We assumed for the MSa the same C, N, O, Mg, Al, and Na abundances of the population "a" of Mi13; for the chemical composition of the MSbc we considered the average of the abundances of the population "b" and "c" listed by Mi13.

As mentioned above, we obtained synthetic spectra for the adopted chemical compositions, integrated them over the transmission curves of the U, B, V, I filters, and computed the helium difference using the best-fitting model.

We obtained that the MSbc is helium enhanced with respect to the MSa of $\Delta Y = 0.025 \pm 0.006$. As for NGC 6121, since the U magnitude is affected by the abundance of light elements, we used $B - I$ and $V - I$ colors only to estimate Y. Note that the abundance of light elements assumed in the model does not affect our conclusion on the helium abundance of the two MSs, as already proven in the case of NGC 6121.

6.3. Relation between HB morphology and Helium abundance

In their work, Milone et al. (2014b) have sought correlations between HB morphology indicators and physical and morphological GC parameters. Among these parameters there is also the maximum helium difference between stellar populations hosted by GCs.

They introduced two different parameters to describe the HB morphology: L_1, which is the color difference between the RGB and the coolest border the HB, and L_2, which is the color

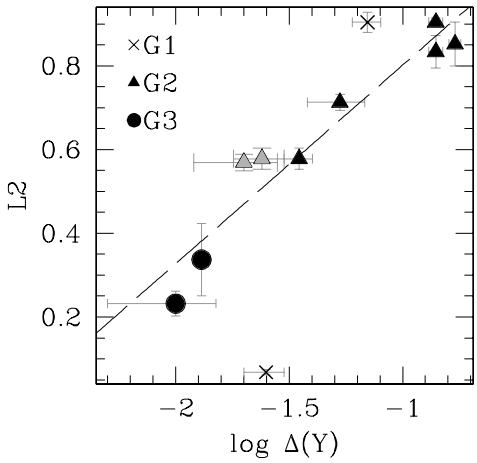

Fig. 17. The HB morphological parameter L_2 as a function of the logarithm of the maximum helium difference among stellar populations in GCs. The black line is the best-fitting straight line for G2+G3 GCs. The data of Milone et al. (2014b) are in black, the data of this work in gray.

Table 5. Parameters used to simulate synthetic spectra of MSa and MSbc stars and estimation of helium difference between the two population for different I_{CUT} in the case of NGC 6752.

I_{CUT}	$T_{EFF,MSa}$	$T_{EFF,MSbc}$	$\log g_{MSa}$	$\log g_{MSbc}$	ΔY
18.55	5410	5456	4.65	4.65	0.021
18.75	5254	5306	4.67	4.67	0.023
18.95	5100	5150	4.69	4.69	0.023
19.15	4946	4998	4.70	4.70	0.025
19.35	4798	4851	4.72	4.72	0.026
Average					0.024, σ = 0.006

extension of the HB (for more details, see Fig. 1 of Milone et al. 2014b).

They divided the sample of 74 GCs in three groups: in the first group, G1, there are GCs with [Fe/H] ≥ -1.0; the second group, G2, includes GCs with [Fe/H] < -1.0 and $L_1 \leq 0.4$; the third group, G3 contains GCs with $L_1 > 0.4$.

They found a tight correlation between L_2 and the maximum internal helium difference (ΔY, measured on the MS) for the group G2+G3 (see Fig. 8 of their paper).

We add two more points to their data set: the helium difference between the two populations of NGC 6752 and NGC 6121, as computed in this work. In the case of NGC 6752, the added point constitutes a lower limit because the helium difference between Pop_a and Pop_{bc}, $\Delta Y(Pop_a - Pop_{bc})$, is the average value between $\Delta Y(Pop_a - Pop_b)$ and $\Delta Y(Pop_a - Pop_c)$.

The result is in Fig. 17: in black there are the points of Milone et al. (2014b) and in gray the points added in this work. In analogy to the work of Milone et al. (2014b), the crosses refer to the G1 GCs, triangles to G2 group and dots to G3 clusters. Our data points confirm the tight correlation between L2 and ΔY. We found a Spearman's rank correlation coefficient $r_{G2+G3} = 0.93$ (to be compared to $r_{G2+G3} = 0.89 \pm 0.17$ found by Milone et al. 2014b), with $\sigma_{r,G2+G3} = 0.08$ (the uncertainty in r is estimated by means of bootstrapping statistic, as in Milone et al. 2014b).

This result is further proof that the helium-enhanced stellar populations are likely related to the HB extension, as predicted by theory.

7. Summary

The photometric analysis of ESO/FORS2 data of the external regions of the three nearby Galactic GCs NGC 6121 (M 4), NGC 6752, and NGC 6397 has confirmed that the first two GCs host multiple stellar populations. Indeed, the B versus $U - B$ and V versus $c_{U,B,I}$ CMDs of NGC 6752 and NGC 6121 show a split of the MS in two components. Excluding the unique case of ω Cen, this is the first time that a split of the MS is observed using ground-based facilities.

The multiple stellar populations of NGC 6397 was investigated by Milone et al. (2012a) using HST data. They found two stellar populations characterized by a modest helium variation $\Delta Y \sim 0.01$. Unfortunately, it was not possible to analyze these populations in this work, because of the size of our photometric errors is comparable to the small color separation between the MSs.

Using HST data, Mi13 have already demonstrated that NGC 6752 host three stellar populations. They computed the radial trend of the ratio between the number of stars of different populations out a radial distance from the center of 6.′13. Because of larger photometric errors, we have resolved only two MSs. Comparing them with the work of Mi13, we found that the less populous MS corresponds to their population "a", while the most populous MS hosts both their populations "b" and "c". On average, we found that the MSa contains about 26% of the total number of stars and the MSbc host about 74% of the MS stars. The most straightforward interpretation is that the MSa is formed by stars of the first generation with chemical abundances similar to that of the Galactic halo field stars with the same metallicity; the MSbc hosts stars of second generation, formed out of material processed through first-generations stars. This population is characterized by stars enhanced in helium, with $\Delta Y = 0.025$. Our measurement of the helium enhancement is in agreement with the average ΔY of the populations "b" ($\Delta Y \sim 0.01$) and "c" ($\Delta Y \sim 0.03$) obtained by Mi13. We extended the study of the radial trend of the populations of NGC 6752 to more external regions, confirming the results of Mi13, of a flat distribution. Therefore we cannot confirm the results by Kravtsov et al. (2011, 2014); they found that the two populations show a strong gradient at a radial distance close to the half-mass radius.

In a recent work on NGC 6121, Milone et al. (2014a) investigate the bottom of the MS of this cluster using HST near-infrared photometry. They found that the MS splits into two sequences below the MS knee. In particular they identified two MSs: a MS_I that contains ~38% of stars and MS_{II} formed by the remaining 62%. They show that the split of the MS is mainly due to the effect of H_2O molecules, present in the atmospheres of M-dwarfs, on their near-infrared color, and that it is possible to associate the MS_I with a first generation of stars and the MS_{II} to a second generation of stars. Marino et al. (2008), analyzing spectra of RGB stars, found that ~64% of stars are Na-rich and O-poor and the remaining ~36% have chemical abundances similar to those of Halo-field stars with the same metallicity. All these results are in agreement with what we have obtained in this work: the MS of NGC 6121 splits in the B versus $(U - B)$ and V versus $c_{U,B,I}$ CMDs. We found two MSs: a less populous MS that contains ~37% of MS stars and constitutes the first generation of stars, and a more populous second generation MS that contains ~63% of stars. Villanova et al. (2012), using spectroscopic measurements of blue HB (bHB) stars, found that the difference in helium abundance between these stars and the red HB (rHB) stars is $\Delta Y = 0.02/0.03$. A spectroscopic analysis of

Marino et al. (2011) revealed that the rHB stars have solar-scaled [Na/Fe], while bHB stars are Na enhanced. In contrast to the results of Villanova et al. (2012), a lower constraint to the level of He enhancement is set by Valcarce et al. (2014), founding a maximum $\Delta Y = 0.01$ between bHB and rHB stars. Analyzing how the two MS of NGC 6121 behave in different CMDs, we computed the helium abundance difference between them. Our result is $\Delta Y = 0.020 \pm 0.005$, in agreement with that obtained by Villanova et al. (2012). Also, in the case of NGC 6121, we did not find evidence of changes in the fraction of bMS/rMS stars in the radial range between $1.2\, r_h < R < 4.1\, r_h$.

Milone et al. (2014b) found a correlation between the HB morphological parameter L_2 and the maximum helium difference among stellar populations in GCs. Using the helium abundances computed in this work for NGC 6121 and NGC 6752, we confirm this correlation and the theoretical indications that helium enhanced stellar populations are responsible for the HB extension.

Acknowledgements. D.N. is supported by a grant "Borsa di studio per l'estero, bando 2013" awarded by "Fondazione Ing. Aldo Gini" in Padua (Italy). A.P.M. acknowledges the financial support from the Australian Research Council through Discovery Project grant DP120100475. A.F.M. has been supported by grants FL110100012 and DP120100991.

References

Anderson, J., Bedin, L. R., Piotto, G., Yadav, R. S., & Bellini, A. 2006, A&A, 454, 1029
Bedin, L. R., Piotto, G., King, I. R., & Anderson, J. 2003, AJ, 126, 247
Bedin, L. R., Piotto, G., Anderson, J., et al. 2004, ApJ, 605, L125
Bekki, K. 2011, MNRAS, 412, 2241
Bell, R. A., Dickens, R. J., & Gustafsson, B. 1979, ApJ, 229, 604
Bellini, A., Piotto, G., Bedin, L. R., et al. 2009a, A&A, 493, 959
Bellini, A., Piotto, G., Bedin, L. R., et al. 2009b, A&A, 507, 1393
Bellini, A., Anderson, J., Salaris, M., et al. 2013a, ApJ, 769, L32
Bellini, A., Piotto, G., Milone, A. P., et al. 2013b, ApJ, 765, 32
Brown, J. A., Wallerstein, G., & Oke, J. B. 1990, AJ, 100, 1561
Carretta, E., Gratton, R. G., Lucatello, S., Bragaglia, A., & Bonifacio, P. 2005, A&A, 433, 597
Carretta, E., Bragaglia, A., Gratton, R. G., Lucatello, S., & Momany, Y. 2007, A&A, 464, 927
Carretta, E., Bragaglia, A., Gratton, R. G., et al. 2009, A&A, 505, 117
Carretta, E., Bragaglia, A., Gratton, R. G., Lucatello, S., & D'Orazi, V. 2012, ApJ, 750, L14
Cassisi, S., Salaris, M., & Pietrinferni, A. 2013, Mem. Soc. Astron. It., 84, 91
Castelli, F. 2005, Mem. Soc. Astron. It. Supp., 8, 25
Cottrell, P. L., & Da Costa, G. S. 1981, ApJ, 245, L79
D'Antona, F., Caloi, V., Montalbán, J., Ventura, P., & Gratton, R. 2002, A&A, 395, 69
D'Ercole, A., Vesperini, E., D'Antona, F., McMillan, S. L. W., & Recchi, S. 2008, MNRAS, 391, 825
di Criscienzo, M., D'Antona, F., & Ventura, P. 2010, A&A, 511, A70
Drake, J. J., Smith, V. V., & Suntzeff, N. B. 1992, ApJ, 395, L95
Freudling, W., Romaniello, M., Patat, F., et al. 2007, in The Future of Photometric, Spectrophotometric and Polarimetric Standardization, ed. C. Sterken, ASP Conf. Ser., 364, 113
Gratton, R. G., Quarta, M. L., & Ortolani, S. 1986, A&A, 169, 208
Gratton, R. G., Bonifacio, P., Bragaglia, A., et al. 2001, A&A, 369, 87
Grundahl, F., Catelan, M., Landsman, W. B., Stetson, P. B., & Andersen, M. I. 1999, ApJ, 524, 242
Grundahl, F., Briley, M., Nissen, P. E., & Feltzing, S. 2002, A&A, 385, L14
Harris, W. E. 1996, AJ, 112, 1487
Ivans, I. I., Sneden, C., Kraft, R. P., et al. 1999, AJ, 118, 1273
King, I. R., Bedin, L. R., Cassisi, S., et al. 2012, AJ, 144, 5
Kravtsov, V., Alcaíno, G., Marconi, G., & Alvarado, F. 2011, A&A, 527, L9
Kravtsov, V., Alcaíno, G., Marconi, G., & Alvarado, F. 2014, ApJ, 783, 56
Kurucz, R. L. 2005, Mem. Soc. Astron. It. Supp., 8, 14
Lee, J.-W., Kang, Y.-W., Lee, J., & Lee, Y.-W. 2009, Nature, 462, 480
Libralato, M., Bellini, A., Bedin, L. R., et al. 2014, A&A, 563, A80
Lind, K., Charbonnel, C., Decressin, T., et al. 2011, A&A, 527, A148
Marino, A. F., Villanova, S., Piotto, G., et al. 2008, A&A, 490, 625
Marino, A. F., Villanova, S., Milone, A. P., et al. 2011, ApJ, 730, L16
Marino, A. F., Milone, A. P., Przybilla, N., et al. 2014, MNRAS, 437, 1609
Milone, A. P., Villanova, S., Bedin, L. R., et al. 2006, A&A, 456, 517
Milone, A. P., Piotto, G., King, I. R., et al. 2010, ApJ, 709, 1183
Milone, A. P., Marino, A. F., Piotto, G., et al. 2012a, ApJ, 745, 27
Milone, A. P., Piotto, G., Bedin, L. R., et al. 2012b, A&A, 540, A16
Milone, A. P., Piotto, G., Bedin, L. R., et al. 2012c, ApJ, 744, 58
Milone, A. P., Marino, A. F., Piotto, G., et al. 2013, ApJ, 767, 120
Milone, A. P., Marino, A. F., Bedin, L. R., et al. 2014a, MNRAS, 439, 1588
Milone, A. P., Marino, A. F., Dotter, A., et al. 2014b, ApJ, 785, 21
Monelli, M., Milone, A. P., Stetson, P. B., et al. 2013, MNRAS, 431, 2126
Norris, J. 1981, ApJ, 248, 177
Norris, J., Cottrell, P. L., Freeman, K. C., & Da Costa, G. S. 1981, ApJ, 244, 205
Pancino, E., Rejkuba, M., Zoccali, M., & Carrera, R. 2010, A&A, 524, A44
Pietrinferni, A., Cassisi, S., Salaris, M., & Castelli, F. 2004, ApJ, 612, 168
Pietrinferni, A., Cassisi, S., Salaris, M., Percival, S., & Ferguson, J. W. 2009, ApJ, 697, 275
Piotto, G., Bedin, L. R., Anderson, J., et al. 2007, ApJ, 661, L53
Piotto, G., Milone, A. P., Anderson, J., et al. 2012, ApJ, 760, 39
Ramírez, S. V., & Cohen, J. G. 2002, AJ, 123, 3277
Sbordone, L., Bonifacio, P., & Castelli, F. 2007, in IAU Symp. 239, eds. F. Kupka, I. Roxburgh, & K. L. Chan, 71
Sbordone, L., Salaris, M., Weiss, A., & Cassisi, S. 2011, A&A, 534, A9
Shen, Z.-X., Bonifacio, P., Pasquini, L., & Zaggia, S. 2010, A&A, 524, L2
Smith, G. H., & Briley, M. M. 2005, PASP, 117, 895
Sollima, A., Ferraro, F. R., Bellazzini, M., et al. 2007, ApJ, 654, 915
Stetson, P. B. 2000, PASP, 112, 925
Valcarce, A. A. R., Catelan, M., Alonso-García, J., Cortés, C., & De Medeiros, J. R. 2014, ApJ, 782, 85
Villanova, S., Piotto, G., & Gratton, R. G. 2009, A&A, 499, 755
Villanova, S., Geisler, D., Piotto, G., & Gratton, R. G. 2012, ApJ, 748, 62
Vesperini, E., McMillan, S. L. W., D'Antona, F., & D'Ercole, A. 2013, MNRAS, 429, 1913
Yong, D., Grundahl, F., Lambert, D. L., Nissen, P. E., & Shetrone, M. D. 2003, A&A, 402, 985
Yong, D., Grundahl, F., Nissen, P. E., Jensen, H. R., & Lambert, D. L. 2005, A&A, 438, 875
Yong, D., Grundahl, F., Johnson, J. A., & Asplund, M. 2008, ApJ, 684, 1159
Yong, D., Meléndez, J., Grundahl, F., et al. 2013, MNRAS, 434, 3542